ACS OMEGA

Open Access



http://pubs.acs.org/journal/acsodf

Article

# Pterostilbene-Isothiocyanate Inhibits Proliferation of Human MG-63 Osteosarcoma Cells via Abrogating β-Catenin/TCF-4 Interaction—A Mechanistic Insight

Viney Kumar, Swati Haldar, Souvik Ghosh, Saakshi Saini, Poonam Dhankhar, and Partha Roy*

Cite This: ACS Omega 2023, 8, 43474−43489

Read Online

ACCESS | Metrics & More | Article Recommendations | Supporting Information

**ABSTRACT:** Osteosarcoma, a highly metastasizing bone neoplasm, is a leading cause of death and disability in children and adolescents worldwide. Osteosarcoma is only suboptimally responsive to surgery and radio- and chemotherapy, that too with adverse side effects. Hence, there is a necessary need for safer alternative therapeutic approaches. This study evaluated the anticancer effects of the semi-synthetic compound, pterostilbene-isothiocyanate (PTER-ITC), on human osteosarcoma MG-63 cells through cytotoxicity, wound-healing, and transwell-migration assays. Results showed that PTER-ITC specifically inhibited the survival, proliferation, and migration of osteosarcoma cells. PTER-ITC induced apoptosis in MG-63 cells by disrupting mitochondrial membrane potential, as evident from the outcomes of different cytological staining. The antimetastatic potential of PTER-ITC was evaluated through immunostaining, RT-qPCR, and immunoblotting. *In silico* (molecular docking and dynamic simulation) and, subsequently, biochemical [co-immunoprecipitation (Co-IP) and luciferase reporter] assays deciphered the underlying mode-of-action of this compound. PTER-ITC increased E-cadherin and reduced N-cadherin levels, thereby facilitating the reversal of epithelial-mesenchymal transition (EMT). It also modulated the expressions of proliferative cell nuclear antigen (PCNA), caspase-3, poly [ADP-ribose] polymerase (PARP-1) and matrix metalloproteinase-2/9 (MMPs-2/9) at transcriptional and translational levels. PTER-ITC interfered with the β-catenin/transcription factor-4 (TCF-4) interaction *in silico* by occupying the β-catenin binding site on TCF-4, confirmed by their reduced physical interactions (Co-IP assay). This inhibited transcriptional activation of TCF-4 by β-catenin (as shown by luciferase reporter assay). In conclusion, PTER-ITC exhibited potent anticancer effects *in vitro* against human osteosarcoma cells by abrogating the β-catenin/TCF-4 interaction. Altogether, this study suggests that PTER-ITC may be regarded as a new approach for osteosarcoma treatment.

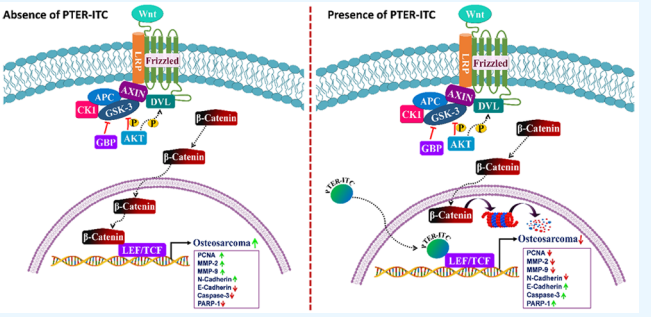


## 1. INTRODUCTION

Osteosarcoma is the most common nonhematological bone tumor among children and adults. In about 80% of all osteosarcomas, osteoblastic cells undergo morphological abnormalities and produce aberrant osteoid structures, leading to poor differentiation at the histopathological level. Osteosarcomas are primarily caused by mesenchymal cells, which typically occur in the distal and upper portions of the bones, resulting in a significant restriction of movement.[1] Lung metastases are responsible for treatment failures and high mortality rates in osteosarcoma.[2]

Although chemotherapy, surgery, and occasional radiotherapy have been used to treat osteosarcoma patients since the 1970s, 5-year survival rates have not improved.[3] Various chemotherapeutic drugs currently used for osteosarcoma are methotrexate, doxorubicin, cisplatin, ifosfamide, etoposide, and zoledronic acid (ZA). This combination of chemotherapeutic drugs has become the standard clinical practice for treating osteosarcoma. It not only eradicates cancer cells more effectively than a single medication but also has a lower chance of failure due to drug resistance. Children, adolescents, and young adults with osteosarcoma are usually treated with methotrexate, doxorubicin, and cisplatin, while older patients are more frequently treated with doxorubicin and cisplatin. These drugs, however, have adverse side effects, like ifosfamide can damage the bladder lining and cisplatin can cause nerve damage (called neuropathy), leading to kidney damage, numbness, tingling, or pain in the hands and feet. Etoposide increases the risk of developing acute myeloid leukemia (AML), and high doses of methotrexate can damage the white matter of the brain (called leukoencephalopathy) and affect the

Received: April 20, 2023
Revised: September 26, 2023
Accepted: October 4, 2023
Published: November 6, 2023

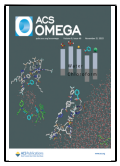

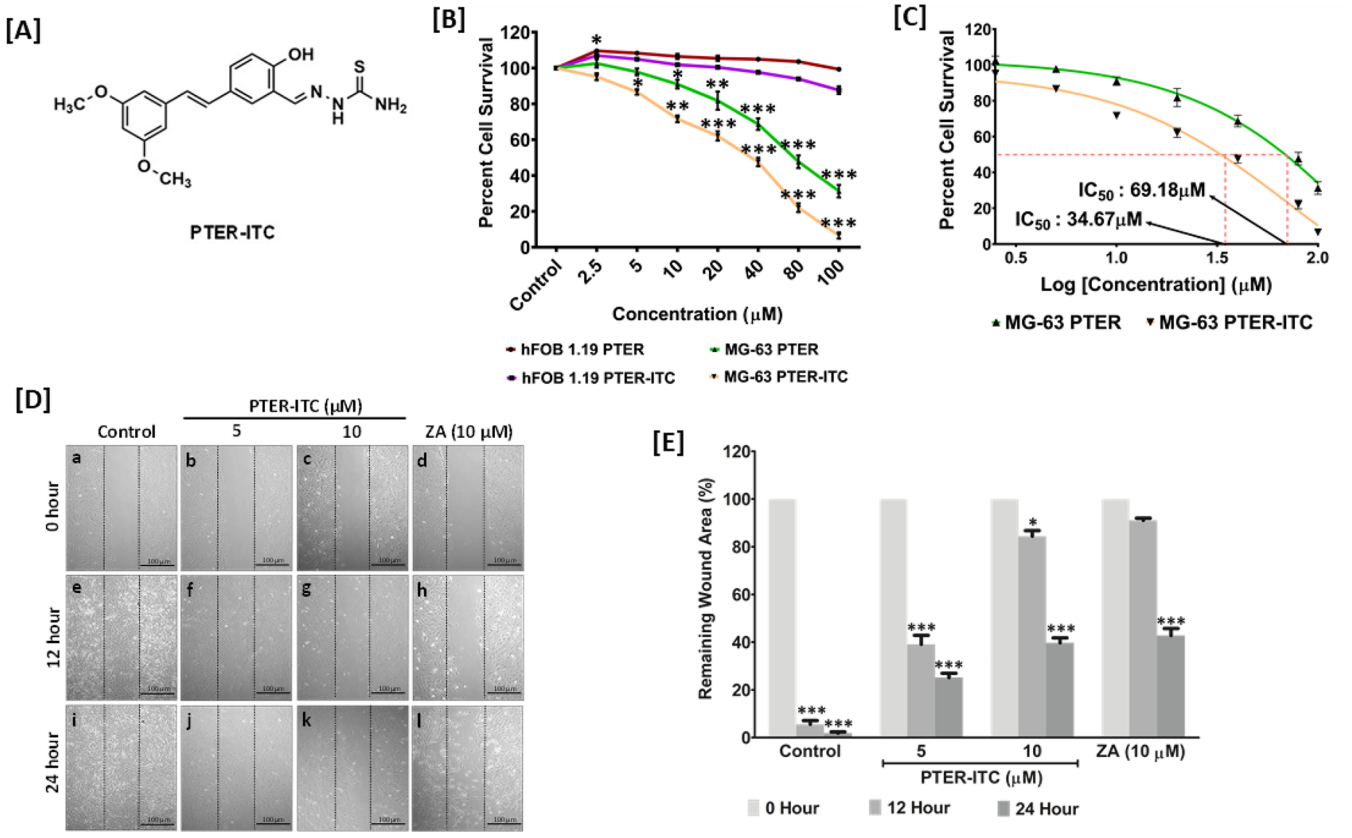


**Figure 1.** PTER-ITC selectively inhibits the proliferation of the MG-63 osteosarcoma cell line. (A) Chemical structure of PTER-ITC. (B) MTT assay depicting the effect of PTER and PTER-ITC on the viability of human normal (hFOB 1.19) and osteosarcoma (MG-63) cell lines. Statistical significance of the difference, denoted as mean ± SE of three independent experiments, observed in the effects of PTER and PTER-ITC treatments on MG-63 cells for corresponding concentrations was determined through one-way ANOVA and indicated with *, ** and *** for $p < 0.05$, 0.01 and 0.001, respectively. (C) Dose−response curves comparatively represent the effects of PTER and PTER-ITC on human osteosarcoma MG-63 cell line. (D) Representative micrographs and (E) corresponding quantification of wound-healing assay depicting the effect of different concentrations (5 and 10 $\mu$M) of PTER-ITC on the proliferation of MG-63 cells over 12 and 24 h. Data represented as mean ± SE of three independent experiments. Statistical significance of the observed effect of PTER-ITC and ZA (positive control) treatments on wound-healing in MG-63 cells was determined through two-way ANOVA and indicated as *, *** for $p < 0.05$ and 0.001 respectively, when compared to 0 h for each experimental group. All data were obtained from three independent experiments. Scale bar: 100 $\mu$m.

liver and kidneys. Doxorubicin can damage the heart muscles (https://www.cancer.org/cancer/osteosarcoma/treating/chemotherapy.html). ZA is the only bisphosphonate approved by the Food and Drug Administration (FDA) with acceptable safety and tolerability for the prevention and treatment of metastatic bone diseases. It still has side effects like osteoporosis-related fractures, renal impairment, and serious atrial fibrillation associated with systemic or direct injection of ZA that limits its clinical use.[1]

The two main causes of osteosarcoma chemotherapy failure and poor prognoses are metastasis and drug resistance.[4] Despite being one of the most effective treatment options in the clinical arena, multidrug resistance (MDR) often hinders the effectiveness of doxorubicin. MDR is assumed to be primarily caused by ATP-binding cassette transporters, such as P-glycoprotein, which pump the drug out of the cancer cells.[5] Anthracyclines are P-glycoprotein substrates that cause MDR and chemotherapy failure, hindering their clinical use.[6] As a result, a new approach to treatment and survival is needed for osteosarcoma patients. Therefore, the combination of two drugs (hybrid drugs) was thought to overcome these limitations to a great extent.

Hybridization is an effective method that combines two different existing molecules to create new multifunctional compounds. The chemodiversity of drug-like molecules can be boosted by combining various bioactive molecules in different combinations.[7] Natural products can be highly effective starting points for developing new drugs. The anticancer drugs currently in use are natural or derived from natural products, which accounts for more than 70%, and this number is expected to rise when combined to form new hybrid compounds.[8,9] These new hybrid compounds' additive or synergistic effects in the treatment of various diseases, particularly cancer therapy,[7] is a promising approach to preventing resistance or finding new applications for treatments in the future.[10] This becomes more pertinent when two phytochemical-based pharmacophores are combined since they are expected to have fewer side effects and better efficacy. Fascinated by this hybrid drug concept, a semi-synthetic compound with multitargeting potential named pterostilbene-isothiocyanate (PTER-ITC) was synthesized (Figure 1A).[11] PTER-ITC was synthesized by conjugating the isothiocyanate (ITC) group to pterostilbene (PTER) at its meta position.[11] The activities of PTER-ITC, like anticancer, antiosteoclastogenic, and antimetastatic, were observed and reported earlier.[11−15]

Several findings indicate that abnormal expression or prolonged activation of Wnt/$\beta$-catenin pathway leads to


https://doi.org/10.1021/acsomega.3c02732
ACS Omega 2023, 8, 43474−43489

osteosarcoma tumorigenesis.[16] Thus, an effective way of treating cancers would be targeting the Wnt/$\beta$-catenin pathway. The current study examined the anticancer effect of PTER-ITC on MG-63 human osteosarcoma cells and confirmed whether it can target the Wnt/$\beta$-catenin signaling pathway. Our observations revealed that PTER-ITC affects MG-63 osteosarcoma cells while being safe on hFOB 1.19 normal bone cells and targets Wnt/$\beta$-catenin signaling by inhibiting the interaction of $\beta$-catenin/transcription factor-4 (TCF-4).

## 2. MATERIAL AND METHODS

**2.1. Cell Lines and Reagents.** Human osteoblast cell line hFOB 1.19 was a kind gift from Prof. Naibedya Chattopadhyay of CSIR-Central Drug Research Institute, Lucknow, India. Human osteosarcoma cell line MG-63 was procured from ATCC recognized cell repository at National Centre for Cell Science (NCCS), Pune, India. Heat inactivated fetal bovine serum (FBS), penicillin-streptomycin antibiotic cocktail, and trypsin-EDTA were purchased from Gibco (Inchinnan, UK). Dulbecco's Modified Eagle's Medium-F12 (DMEM-F12) (catalog # AT106), minimal essential medium with alpha modification ($\alpha$-MEM) (catalog # AT154), 3-[4,5-dimethylthiazol-2-yl]2,5-diphenyl tetrazolium bromide (MTT) (catalog # TC191), Bovine serum albumin (BSA) (catalog # TC194), acridine orange (AO) (catalog # MB116), ethidium bromide (catalog # MB071), and 4′,6-diamidino-2-phenylindole dihydrochloride (DAPI) (catalog # MB097) were procured from Himedia (Mumbai, India). Rhodamine 123 (catalog # 16672) was procured from Cayman Chemicals (Michigan, USA). ZA (catalog no. SML0223) was purchased from Sigma-Aldrich (Missouri, USA). Terminal deoxynucleotidyl transferase dUTP nick end labeling (TUNEL) assay kit (catalog # 22853) was procured from AAT Bioquest (California, USA). Antibodies against proliferative cell nuclear antigen (PCNA) (E-AB-10010), cleaved poly [ADP-ribose] polymerase-1 (PARP-1) (E-AB-30059), matrix metalloproteinase-2 (MMP-2) (E-AB-32054), matrix metalloproteinase-9 (MMP-9) (E-AB-70247), active Caspase-3 (E-AB-22115), TCF-4 (E-AB-60206), and $\beta$-actin (E-AB-20058) were purchased from Elabscience (Texas, USA). Antibodies against E-cadherin (Sc-8426), N-cadherin (Sc-8424) and $\beta$-catenin (Sc-7963) were procured from Santa Cruz Biotechnology (Texas, USA). The HRP-conjugated anti-mouse (catalog # 115-035-003/111) and anti-rabbit (catalog # 111-035-003/111) secondary antibodies were purchased from Jackson ImmunoResearch Laboratory (Pennsylvania, USA). Goat anti-mouse FITC conjugated (catalog # 62−6511) and goat anti-mouse TRITC conjugated (catalog # A16071) secondary antibodies were procured from Thermo Fisher Scientific (Massachusetts, USA). Reverse transcriptase (catalog # EP0441) and RT-qPCR SYBR green master mix (catalog # K0221) were procured from Thermo Fisher Scientific (Massachusetts, USA). Protein A-sepharose beads (catalog # 786−283) were procured from G Biosciences (Missouri, USA). Polyfect transfection reagent (catalog # 301105) was procured from Qiagen Inc. (California, USA). All primers were synthesized from Eurofins Scientific (Luxembourg, Europe). Analytical grade methanol, chloroform, and dimethyl sulfoxide (DMSO) were procured from Sisco Research Laboratories (Mumbai, India). PTER and PTER-ITC was synthesized in-house, according to a procedure described in an article published earlier from our laboratory.[11]

**2.2. Cell Culture.** hFOB 1.19 cells were cultured in DMEM-F12 culture medium with G418 (0.3 mg/mL), 2.5 mM L-glutamine, and 10% FBS at 34 °C. The MG-63 cells were maintained in $\alpha$-MEM medium supplemented with 10% FBS and 1% antibiotic (100 U/mL of penicillin and 100 $\mu$g/mL streptomycin) cocktail, at 37 °C in a humidified incubator with 5% carbon dioxide ($CO_2$) in the atmosphere.

**2.3. Cytotoxicity Assay.** MTT assay was performed according to a previously published protocol.[15] Cell survival assays were conducted on hFOB 1.19 and MG-63 cell lines to evaluate the effects of PTER and PTER-ITC on cell viability. The assay was done in 96-well plates, and cells were seeded at least 24 h before initiating the assay. Different dilutions of PTER and PTER-ITC (2.5, 5, 10, 20, 40, 80, and 100 $\mu$M), dissolved in DMSO, were then added to the cells. The cell survival was assayed after 24 h by adding 20 $\mu$L of 5 mg/mL MTT and incubating for another 4 h at 37 °C for formazan crystals to develop. Then, the MTT-containing medium was removed, and 200 $\mu$L of DMSO was added to dissolve the water-insoluble formazan crystals. The absorbance was measured in a microplate reader (Fluostar optima, BMG Labtech, Ortenberg, Germany) at 570 nm. Percent cell viability was calculated from the obtained absorbance using the following formula.

$$\text{Percent cell viability} = \frac{(\text{Absorbance of treated cells} - \text{Absorbance of blank})}{(\text{Absorbance of control} - \text{Absorbance of blank})} \times 100$$

**2.4. Wound-Healing Assay.** The effect of PTER-ITC on cell proliferation was checked through the wound-healing assay according to the methods reported earlier.[17,18] Briefly, the human osteosarcoma MG-63 cell line was grown to 90% confluency in 6-well tissue culture plates. The medium was then removed, and uniform diametric scratches were made on the confluent monolayers using sterile micropipette tips. The monolayers were rinsed with 1X PBS to remove the detached cells and treated with PTER-ITC (5 and 10 $\mu$M) and ZA (10 $\mu$M). The cells were then imaged after 12 and 24 h under a bright-field microscope (Zeiss, Axiovert 25, Jena, Germany). The wound closure was measured using ImageJ software (imagej.nih.gov)[18] and represented graphically as a percentage of the remaining wound area.

**2.5. Immunostaining and Fluorescence Imaging.** MG-63 cells grown on poly-L-lysine coated coverslips were treated with 0.1% DMSO (vehicle control), PTER-ITC or ZA for 24 h. The cells were then fixed with 4% paraformaldehyde, permeabilized with 0.1% Triton X-100 (only for intracellular proteins), blocked in 5% BSA, and incubated independently with primary antibodies against E-cadherin, N-cadherin, $\beta$-catenin, and TCF-4. The anti-mouse/rabbit FITC/TRITC conjugated secondary antibody, as per the requirement, was used to counterstain for visualization. The cells were then imaged under a fluorescence microscope (BioTek Lionheart LX Automated Microscope, Vermont, USA) after staining nuclei with DAPI (0.5 $\mu$g/mL for 10 min in the dark).

**2.6. *In Vitro* Cell Migration Assay.** *In vitro* cell migration assay was carried out according to a previously published protocol[19] with MG-63 cells to evaluate their migration using transwell. For migration assay, $1.25 \times 10^5$ MG-63 cells were seeded on the apical surface of a transwell (24-well insert; pore size, 8 $\mu$m, Corning, New York, USA) in serum-free cell culture media. The baso-lateral chamber was supplied with a


https://doi.org/10.1021/acsomega.3c02732
ACS Omega 2023, 8, 43474−43489

serum-containing media to serve as a chemo-attractant. The cells, grown to 60−70% confluency, were either treated with PTER-ITC or ZA for 24 h. Thereafter, the membranes were fixed in 70% ethanol and stained with 0.2% crystal violet (Himedia, Mumbai, India) for 5 min. After 5 min, the stain was removed and the transwell was washed thrice with 1X PBS. Then, the nonmigrated cells were removed carefully from the apical surface of the membrane, before imaging the migrated ones, adhering to the basolateral surface under a brightfield microscope (BioTek Lionheart LX Automated Microscope, Vermont, USA). The migration was quantified by extracting the stain using 33% glacial acetic acid (SRL, Gurugram, India) and measuring the absorbance of the resulting solution at 578 nm in a microplate reader (Fluostar optima, BMG Labtech, Ortenberg, Germany).

**2.7. Mitochondrial Membrane Potential Integrity Assay.** Rhodamine 123 is a mitochondrial membrane-potential-sensitive and cationic fluorophore that accumulates in living cells and hence used for detecting the mitochondrial membrane potential. Briefly, $2 \times 10^4$ MG-63 cells were seeded in 6-well plates and allowed to grow until 70% confluency. Thereafter the cells were treated with PTER-ITC or ZA for 24 h. Post incubation, the culture medium was aspirated and cells were washed three times with 1X PBS. Subsequently, the cells were incubated in the Rhodamine-labeling (10 $\mu$g/mL) solution for 20−25 min at 37 C. The mitochondrial green fluorescent labeling solution was aspirated, and the cells were rinsed three times in 1X PBS. The mitochondrial green fluorescence was observed under a fluorescence microscope (BioTek Lionheart LX Automated Microscope, Vermont, USA). The resulting fluorescence intensity was quantified using imageJ software.[20]

**2.8. TUNEL Assay.** To detect DNA fragmentation after treatment with PTER-ITC or ZA, TUNEL assay was performed as per manufacturer's protocol. Briefly, after treatment, the cells were washed with 1× PBS twice, followed by fixation with 4% paraformaldehyde and incubation for 30 min on ice. After fixation, paraformaldehyde was removed from the cells and washed with 1X PBS thrice. Subsequently, 100 $\mu$L of ice-cold 70% ethanol was added to the cells, and the samples were incubated for 1 h on ice. Subsequently, alcohol was removed, cells washed with 1X PBS twice, resuspended in 50 $\mu$L of terminal deoxynucleotidyl transferase (TdT) staining solution (45 $\mu$L of TdT Reaction Buffer; 5 $\mu$L of $CoCl_2$; 0.5 $\mu$L of TF5-dUTP; 0.5 $\mu$L of TdT enzyme) and incubated for 2 h at 37 °C. The TdT staining solution was removed post-incubation and the cells were washed with 1X PBS. Fresh 1× PBS was then added to the cells and imaged under a fluorescence microscope (BioTek Lionheart LX Automated Microscope, Vermont, USA). The fluorescence intensity of individual cells was measured using imageJ software.[20]

**2.9. DAPI and Acridine Orange/Ethidium Bromide (AO/EtBr) Staining.** Morphological indication of apoptosis was determined by DAPI and AO/EtBr staining. This staining helps to visualize the differences between healthy and apoptotic/necrotic cells. Approximately, $5 \times 10^5$ cells were seeded in a 6-well plate and grown up to 60% confluency. After treatment with PTER-ITC or ZA for 24 h, the cells were washed with 1× PBS and fixed with 4% formaldehyde. Subsequently, 500 $\mu$L of AO/EtBr dye mixture (100 $\mu$g/mL AO and 100 $\mu$g/mL EtBr) was added and incubated for 10 min. A parallel set of identically treated cells were stained with DAPI. The stains were then removed and washed with 1× PBS. Thereafter, the cells were observed under a fluorescent microscope (BioTek Lionheart LX Automated Microscope, Vermont, USA).

**2.10. RT-qPCR Analysis.** RT-qPCR analyses of *PCNA*, *PARP-1*, *Caspase-3*, *MMP-2*, *MMP-9*, *E-cadherin*, *N-cadherin*, *β-catenin,* and *TCF-4* were conducted with SYBR Green Master Mix (Thermo Fisher, Massachusetts, USA) according to the manufacturer's protocol using Quant Studio 3 (Applied Biosystems, Massachusetts, USA). *β-actin* gene was included as an internal control. The data were acquired using built-in software, and relative expression was calculated through the $\Delta\Delta C_t$ method. The sequences of the primers used in this study are listed in Table 1.

**Table 1. List of Primers Used in This Study**

| Primer[a] | Sequence (5′− 3′) |
|---|---|
| *β*-actin For | CTCCATCGTCCACCGCAA |
| *β*-actin Rev | GTCACCTTCACCGTTCCAG |
| PCNA For | GTGAACCTCACCAGTATGTCC |
| PCNA Rev | GCTGAGATCTCGGCATATACG |
| E-cadherin For | GAGGAGAGCGGTGGTCAAAGAG |
| E-cadherin Rev | CCTGTGCAGCTGGCTCAAGTCAA |
| N-cadherin For | CAGTAAGCACAGTGGCCACCTAC |
| N-cadherin Rev | GCTCCTGGCCCAGTTACACTGT |
| MMP-2 For | TGCGGCACCACTGAGGACTACGAC |
| MMP-2 Rev | TCCGGGAGCTCAGGCCAGAATGT |
| MMP-9 For | CGCGGGCGGTGATTGACGAC |
| MMP-9 Rev | GTGGTGCAGGCGGAGTAGGATTGG |
| Caspase-3 For | GGTTCATCCAGTCGCTTTGTG |
| Caspase-3 Rev | GCGTCAAAGGAAAAGGACTCA |
| PARP-1 For | CCCAGGGTCTTCGGATAG |
| PARP-1 Rev | AGCGTGCTTCAGTTCATACA |
| *β*-catenin For | GGTCCTCTGTGAACTTGCTCAGG |
| *β*-catenin Rev | GTGGCTTGTCCTCAGACATTCGG |
| TCF-4 For | CCATCACACTCCTCAGCAGA |
| TCF-4 Rev | TTTCCCCAGAGCATCTCCAG |

[a]For, Forward; Rev, Reverse.

**2.11. Protein Expression and Immunoblot Analysis.** The effect of PTER-ITC treatment on protein levels of PCNA, PARP-1, Caspase-3, MMP-2, MMP-9, E-cadherin, and N-cadherin were checked through immunoblot, according to an earlier published protocol.[15] The cell lysates prepared in RIPA buffer [50 mM Tris pH 8, 150 mM NaCl, 1% Na-deoxycholate, 1% NP-40, 5 mM EDTA, 0.1% SDS, 1 mM PMSF, and 1× protease inhibitor cocktail (Sigma-Aldrich, Missouri, USA)], were resolved on denaturing polyacrylamide gel and subsequently, transferred onto 0.2 $\mu$m PVDF membrane (catalog # SVFX8301XXXX101, Advanced Micro-devices Pvt. Ltd., Ambala, India). The membranes were then blocked with 5% nonfat skim milk and probed sequentially with primary (1:1000) and compatible secondary antibodies (1:5000). Finally, the blot was developed through the electrochemiluminescent (ECL) method using luminol reagents (Bio-Rad Laboratories, California, USA). *β*-actin was used as a loading control.

**2.12. *In Silico* Studies.** *2.12.1. Molecular Docking.* The crystal structure of *β*-catenin with TCF-4 was retrieved from RCSB Protein data bank (PDB ID:1JDH).[21] The affinity of PTER-ITC for TCF-4 was assessed by molecular docking using AutoDock Tools.[22] The structure of TCF-4 was prepared for molecular docking by the addition of hydrogen


https://doi.org/10.1021/acsomega.3c02732
ACS Omega 2023, 8, 43474−43489

atoms using MGL Tools. PTER-ITC was drawn with ACD/ChemSketch and the 3D structure was generated using Avogadro21.90.0. The energy was minimized by universal force field (UFF) and converted to pdbqt format using Open Babel in Pyrx0.8 for docking.[23] The active site of TCF-4 was predicted from published literature as the protein structure is reported in a complex form with β-catenin.[24] The molecular grid box was formed at the interacting active site residues (Gly13, Ala14, Asp16, Glu17, Ile19, Phe21, Glu29) known to be important for β-catenin/TCF-4 interaction.[21,24] The grid box was centered at $X$ = 106.923, $Y$ = 7.263, and $Z$ = 2.557, keeping the dimensions as $X$ = 60, $Y$ = 62, and $Z$ = 34 with a default grid spacing of 0.397 Å and exhaustiveness of 8. The Lamarckian genetic algorithm (LGA) was utilized for molecular docking, and a total of 100 conformations were generated. All the conformations of PTER-ITC were analyzed in PyMOL and the best conformation was selected based on the docking. The interaction figures were analyzed, visualized, and prepared using PyMOL and Maestro (53, Schrödinger Release 2017−4: Maestro, Schrödinger, LLC, New York, NY, 2017).[25]

*2.12.2. Molecular Dynamic (MD) Simulation.* The atomistic binding stability of protein with ligands was investigated using MD simulation. To assess the stability of PTER-ITC/TCF-4 complex, molecular dynamics simulation was conducted using GROningen MAchine for chemical simulations (GROMACS) on an online NMRbox computing platform.[26−28] The topology files of PTER-ITC were generated by PRODRG.[29] The protein complex was solvated in a triclinic box, along with simple point charges (SPC). The volume of the box was 209.08 $nm^3$ and the minimum distance between the edges of the box and the protein was set at 1.0 nm. Positive charges on the systems were neutralized by additions of counterions (6 $Na^+$) and energy was minimized by 50,000 steps with the steepest descent algorithm, as previously reported.[30] The systems were equilibrated for the constant number of particles, volume, and temperature (NVT) and number of particles, pressure, and temperature (NPT) for 1 nanosecond (ns) as reported earlier by Dhankhar et al.[31] During NVT and NPT, temperature (300 K) and pressure (1 bar) were maintained by the Berendsen temperature coupling method and Parrinello−Rahman pressure coupling method.[32,33] The molecular dynamics was run for 100 ns, and the generated trajectory files were saved at every 10 picosecond (ps). The molecular dynamics simulation trajectory was used to generate the root-mean-square deviation (RMSD), radius of gyration ($R_g$), solvent-accessible surface area (SASA), number of hydrogen bonds, and hydrogen bond distribution results.

**2.13. Co-Immunoprecipitation (Co-IP) Assay.** After PTER-ITC treatment, physical interaction between β-catenin and TCF-4 within the cells was checked by a Co-IP assay. Briefly, the extracted protein was immunoprecipitated with β-catenin or TCF-4 antibodies (1:100) individually and then coupled to protein A-Sepharose beads. Immunoprecipitated fractions were then immunoblotted with TCF-4 and β-catenin antibodies, respectively. Inputs were immunoblotted with β-catenin, TCF-4, and β-actin antibodies (1:1000).

**2.14. TOPFlash Luciferase Assay.** M50 Super 8x TOPFlash (Addgene #12456) plasmid was procured from Addgene (Massachusetts, USA). This plasmid contains three tandem TCF consensus binding sites upstream of luciferase reporter gene[34] and therefore used for TCF transcriptional activation assays. To determine whether PTER-ITC prevents β-catenin binding to TCF-4, MG-63 cells were seeded in a 24-well plate and then co-transfected with 450 ng/well of M50 Super 8x TOPFlash plasmid and 0.6 ng/well of β-galactosidase internal control plasmid using Polyfect transfection reagent according to the manufacturer's protocol. After the cells were incubated for 4 h with transfection mix, the previous media was replaced with fresh media and treated with different concentrations of PTER-ITC for 24 h. On completion of the treatment, the cells were lysed with the lysis buffer (0.6 M NaCl, 0.1 M EDTA, 0.2 M $MgSO_4$, 0.2 M DTT, 0.1% Triton X-100, 0.08 M Tricine), and the luminescence was measured using luciferin as a substrate. The value of the luciferase activity for each lysate was normalized to the β-galactosidase activity. Change in luminescence in response to PTER-ITC treatment was expressed as the fold change over control.

**2.15. Statistical Analysis.** All quantitative data was represented graphically using GraphPad Prism 5.04 software (Graph Pad Software, San Diego, California, USA). The in-built analysis option of the software was used to evaluate the statistical significance of the obtained data. Comparison of a single parameter across more than two groups was done using one-way analysis of variance (ANOVA), whereas for more than one parameter, across multiple groups, two-way ANOVA was applied. Statistical analyses were carried out at a 95% confidence level with statistical probability ($p$-value) < 0.05, being considered as significant.

## 3. RESULTS

**3.1. PTER-ITC Selectively Reduced the Viability and Proliferation of MG-63 Osteosarcoma Cells.** Osteosarcoma, like other cancers, is defined as uncontrolled cell proliferation. MTT assay was performed with PTER and PTER-ITC treated normal hFOB 1.19 and cancerous MG-63 cells to evaluate the anticancer effect of PTER-ITC against osteosarcoma (Figure 1B). None of the compounds was found to be cytotoxic for the normal hFOB 1.19 cells, whereas both PTER and PTER-ITC were cytotoxic for cancerous MG-63 cells. Interestingly, PTER-ITC reduced the MG-63 cell viability more effectively than did PTER for subsequent concentrations. This observation was further confirmed by the nonlinear regression analysis, which showed the half-maximal inhibitory concentration ($IC_{50}$) of PTER and PTER-ITC against MG-63 cells to be 69.18 and 34.67 μM, respectively (Figure 1C). Subsequent experiments were conducted with sub-$IC_{50}$ concentrations of PTER-ITC, i.e., 5 and/or 10 μM. Untreated and ZA-treated MG-63 cells were considered negative and positive controls, respectively. An effective concentration of ZA (positive control) (10 μM) against human osteosarcoma MG-63 cells was used as per an earlier published article.[35] Wound-healing assay was performed to analyze the effects of PTER-ITC on cell proliferation (Figure 1D and E). Similar dimensions wound were created in the MG-63 monolayers of each experimental group (Figure 1D, a−d). Untreated control MG-63 cells showed approximately 90% wound-healing within 12 h (Figure 1De and E). The remaining unhealed area showed complete wound closure after 24 h (Figure 1Di and E). At 5 μM PTER-ITC treatment, about 40 and 25% of wound areas were left uncovered after 12 and 24 h, respectively ((Figure 1Df, j and E). At 10 μM PTER-ITC treatment, about 80 and 40% wound area was remained uncovered, after 12 h (Figure 1Dg and E) and 24 h (Figure 1Dk and E), respectively. Altogether, these observations showed that PTER-ITC selectively reduced the viability of


https://doi.org/10.1021/acsomega.3c02732
ACS Omega 2023, 8, 43474−43489

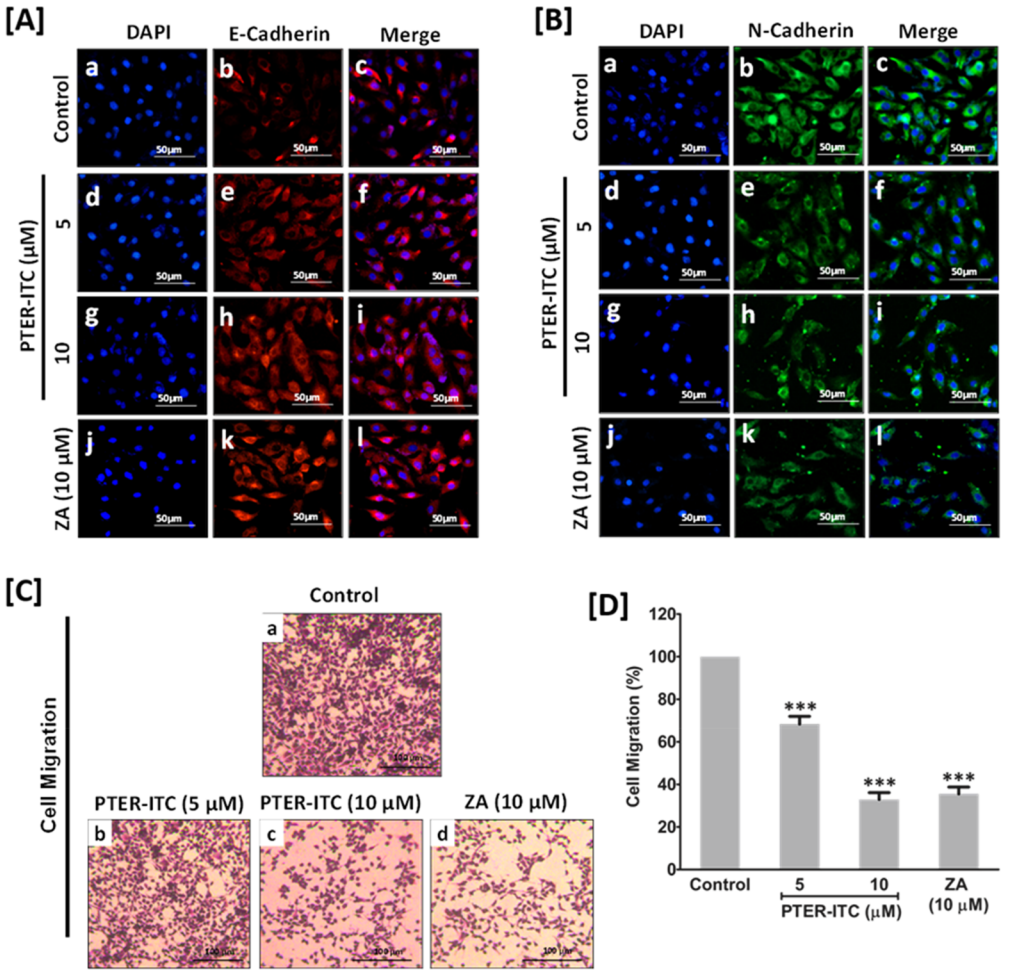


**Figure 2.** Antimetastatic activity of PTER-ITC for human osteosarcoma MG-63 cells. (A, B) Representative immunofluorescent micrographs of (A) antimetastatic E-cadherin and (B) pro-metastatic N-cadherin markers depicting the effects of PTER-ITC (d–i) and ZA (j–l) treatments on MG-63 cells. (a–c) Untreated immunostained MG-63 cells were included as control. Scale bar: 50 $\mu$m. (C) Representative micrographs showing migration of (a) untreated control, (b, c) PTER-ITC-treated, (d) and ZA-treated MG-63 cells and (D) its corresponding quantitative representation. Scale bar: 100 $\mu$m. Data represented as mean ± SE of three independent experiments. Statistical significance of the difference in cell migration observed for different treatment groups was determined through one-way ANOVA and indicated as *** for $p < 0.001$ when compared to untreated control group. For all observations, data were obtained from three independent experiments.

cancerous MG-63 cells and inhibited their proliferation according to the dosage. In addition, PTER-ITC effectively suppressed the viability of cancerous cells. The wound-healing assay showed MG-63 cells as highly proliferative with the metastatic phenotype.[36] As a result, in subsequent experiments, the possible effect of only PTER-ITC on the metastatic phenotype of MG-63 cells was evaluated.

**3.2. PTER-ITC Restrains Metastatic Behavior of MG-63 Osteosarcoma Cells.** Metastasis is characterized by "cadherin-switching", in which E-cadherin is significantly reduced and N-cadherin is increased.[37] To confirm the PTER-ITC's antimetastatic activity against MG-63 osteosarcoma cells, the levels of these E/N-cadherins were assessed by immunofluorescence (Figure 2A and B). A known antimetastatic compound, ZA,[38] was used as a positive control. The expression of E-cadherin in MG-63 cells was visibly less compared to PTER-ITC, and ZA-treated cells, as shown in the representative immunofluorescent micrographs (Figure 2A, a–c). PTER-ITC (Figure 2A, d–i) and ZA (Figure 2A, j–l) treated cells displayed significantly higher E-cadherin levels in the micrographs. On the other hand, contrasting observations were observed with N-cadherin immunofluorescence expression. N-cadherin expression (Figure 2B, a–c) was higher in the untreated cells, compared to PTER-ITC exposed cells (Figure 2B, d–i), where it was significantly lower. Similar reductions in N-cadherin expression were observed with ZA treatment (Figure 2B, j–l). It was evident that PTER-ITC reversed the cadherin-switching in metastatic MG-63 osteosarcoma cells.

The ability of metastatic cells to migrate is also an important feature.[36] Therefore, we evaluated the antimigratory effects of PTER-ITC on MG-63 cells using the transwell migration assay (Figure 2C and D). As shown in the crystal-violet-stained micrograph (Figure 2Ca) and the colorimetric quantification of percent cell migration (Figure 2D), untreated control cells efficiently migrated to the basolateral surface of the transwell. PTER-ITC inhibited the migratory behavior of metastatic MG-63 osteosarcoma cells in a dose-dependent manner (Figure 2Cb and c), with treatments of 5 and 10 $\mu$M PTER-ITC resulting in ~25 ($p < 0.001$) and 70% ($p < 0.001$) decrease in crystal-violet staining, respectively (Figure 2D). In fact, 10 $\mu$M PTER-ITC reduced cell migration as efficiently as the antimetastatic positive control, ZA treatment (Figure 2C c vs d and 2D), bringing the cell responses to both PTER-ITC and ZA's inhibition of cell migration to less than 40%. These


https://doi.org/10.1021/acsomega.3c02732
ACS Omega 2023, 8, 43474–43489

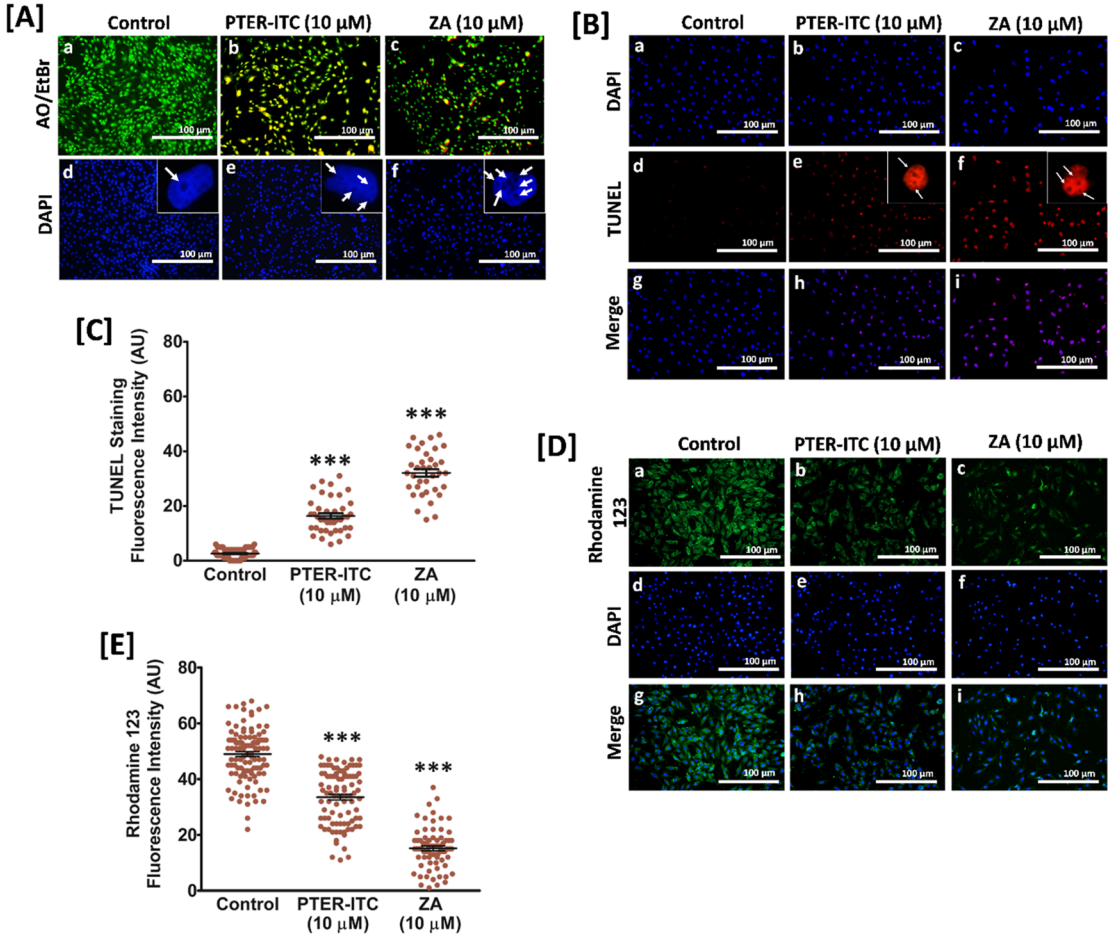


**Figure 3.** PTER-ITC induced apoptosis in MG-63 cells. (A) Representative (a−c) AO/EtBr and (d−f) DAPI-stained micrographs of MG-63 cells depicting the apoptotic effect of (b, e) PTER-ITC and (c, f) ZA treatments. (a, d) Untreated MG-63 cells were included as control. Scale bar: 100 $\mu$m. Insets depict digitally zoomed DAPI-stained nuclei showing (d) intact and (e, f) fragmented (white arrows) nucleolus. (B) Representative micrographs of (a−c) DAPI and (d−f) TUNEL stained cells, and their corresponding merged versions (g−i), demonstrating the apoptotic attribute of PTER-ITC and positive control, ZA. Scale bar: 100 $\mu$m. Insets depict TUNEL-stained nuclei with nucleolar fragmentation indicated through white arrows. (C) Quantitative representation of the outcomes of TUNEL staining shown in (B) as a scatter plot. (D) Representative (a−c) Rhodamine 123 and (d−f) DAPI micrographs, and (g−i) their merged versions showing the effects of PTER-ITC and ZA treatments on the mitochondrial membrane potential of MG-63 cells. Scale bar: 100 $\mu$m. (E) Scatter plot quantitatively representing the outcomes of (D). Data represented as mean ± SE of three independent experiments. Statistical significance of the data represented in (C) and (E) was determined through one-way ANOVA and indicated as *** for $p < 0.001$ when compared to corresponding untreated control groups. All experiments were repeated three times.

observations confirmed the antimetastatic potential of PTER-ITC against MG-63 osteosarcoma cells.

**3.3. PTER-ITC Facilitates Apoptosis in MG-63 Osteosarcoma Cells.** Apoptosis is the mechanism by which cells destroy themselves. Inducing cancer cells to deform and initiate programmed cell death is a key process of molecular-targeted treatment to eliminate the tumor cells. In addition to aberrant cell division and abnormal differentiation, an imbalance in cell apoptosis has been linked to the development and spread of osteosarcoma.[39] Therefore, the apoptosis-inducing potential of PTER-ITC was evaluated. According to the results of live−dead cell staining with AO/EtBr, PTER-ITC did trigger apoptosis as efficiently as the positive control, ZA (Figure 3A, a−c). This was further supported by observing nucleolar fragmentation in DAPI-stained nuclei (Figure 3A, d−f). TUNEL staining was used to confirm that PTER-ITC and ZA treatments caused apoptosis of MG-63 cells, (Figure 3B). The fluorescence intensity from the fluorophore-conjugated deoxynucleotides incorporated in the DNA breaks increased nearly 20-fold ($p < 0.001$) in comparison to the control after PTER-ITC treatment, indicating a considerable increase in DNA fragmentation (Figure 3C). This change was like that of ZA, which exhibited around 30-fold increase in fluorescence intensity ($p < 0.001$) (Figure 3C). The intrinsic pathways of apoptosis are regulated by mitochondria, and during apoptosis, mitochondrial dysfunction or a decrease in mitochondrial membrane potential occur, which ultimately leads to cell death.[40] By dispersing the negative potential along the inner side of the mitochondrial membrane, the cationic fluorescent dye Rhodamine 123 marks the respiring mitochondria. Apoptotic cells' mitochondria are less efficiently stained by Rhodamine 123 because apoptosis causes a decrease in mitochondrial membrane potential. In PTER-ITC and ZA-treated cells compared to the untreated control, specific mitochondrial staining with Rhodamine 123 showed a nearly 0.3 ($p < 0.001$) and 0.68- fold ($p < 0.001$) reduction in fluorescence intensities, respectively. These results demonstrated that both treatments decreased the mitochondrial


https://doi.org/10.1021/acsomega.3c02732
ACS Omega 2023, 8, 43474−43489

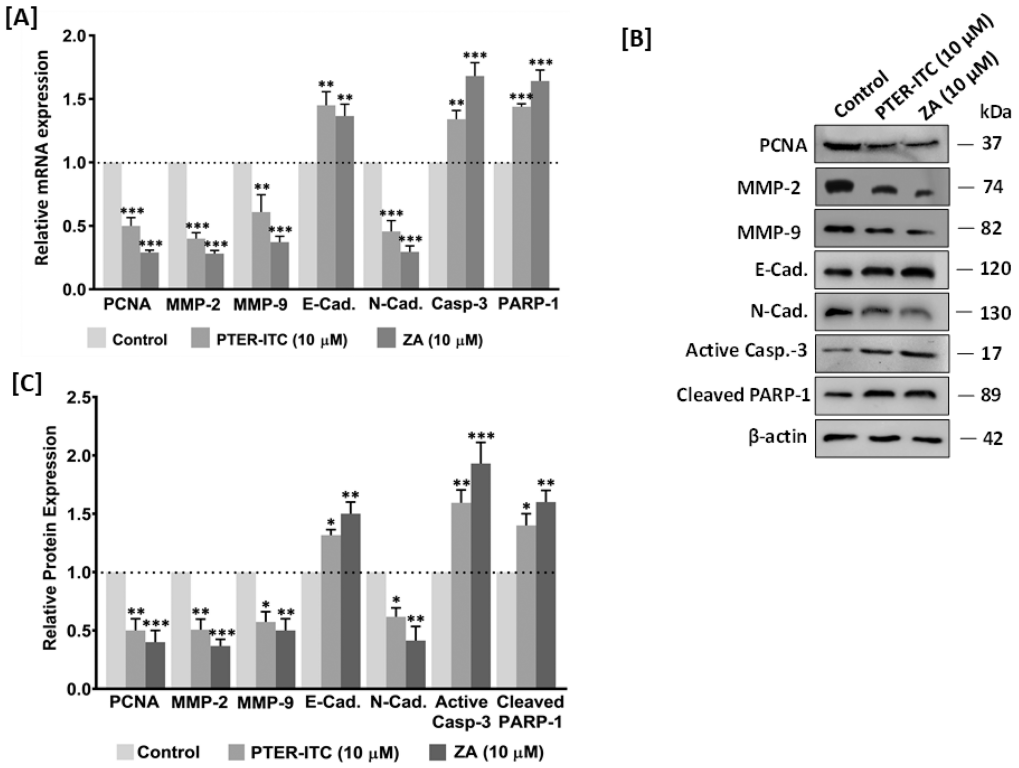


**Figure 4.** Effect of PTER-ITC on transcription and translation of different factors. (A) Effect of PTER-ITC on transcription level of proliferation (*PCNA*), migration (*MMP-2/9*), metastatic (*E/N-cadherin*), and apoptotic (*Caspase-3* and *PARP-1*) markers. (B, C) Representative immunoblot images showing the effect of PTER-ITC and ZA treatments on PCNA, MMP-2/9, E/N-cadherin, active Caspase-3, and cleaved PARP-1 markers (B) along with their corresponding quantitative densitometric analysis (C). Data represented as mean ± SE of three independent experiments. Statistical significance was determined through two-way ANOVA and represented as *, **, and *** for $p < 0.05$, 0.01, and 0.001, respectively, when compared to respective control.

membrane potential (Figure 3D and E). These observations collectively confirmed that PTER-ITC induced apoptosis in MG-63 osteosarcoma cells.

**3.4. PTER-ITC Modulates Different Factors at Transcriptional and Translational Levels.** The mRNA and protein levels of the proliferation marker, PCNA, were used to assess the molecular target of the antiproliferative property of PTER-ITC on MG-63 cells (Figure 4A−C). When compared to the control mRNA expression of PCNA in PTER-ITC-treated cells was nearly half ($p < 0.001$) lower than in the control group (Figure 4A), which was similarly reflected in lower protein levels (Figure 4B and C). Comparable to their ZA-treated counterparts, PTER-ITC-treated cells showed decreased PCNA expression (mRNA and protein) (Figure 4A−C).

High expression of MMPs, especially MMP-2/9, cause the extracellular matrix (ECM) to degrade, which impairs matrix anchoring and reduces cell adhesion, a necessary condition for metastasis.[41] Therefore, the effect of PTER-ITC treatment on MMP-2/9 mRNA and protein levels were evaluated for a better understanding of its antimetastatic property. A significant visible reduction in the mRNA expressions of MMP-2 (∼ 0.6-fold; $p < 0.001$) and MMP-9 (∼ 0.4-fold; $p < 0.01$) (Figure 4A) was observed with PTER-ITC treatment compared to untreated control. These reductions were close to like that of with ZA. The effect of PTER-ITC on MMP-2/9 protein levels was consistent with the corresponding mRNA levels, as evident from ∼0.5 ($p < 0.01$) and 0.45 ($p < 0.05$) folds decrease in MMP-2 and MMP-9 expression levels, respectively, after PTER-ITC treatment, relative to control (Figure 4B and C).

Following PTER-ITC and ZA treatments, RT-qPCR results demonstrated an increase in E-cadherin transcription of about 0.45 ($p < 0.01$) and 0.36 ($p < 0.01$) folds respectively. Likewise, PTER-ITC and ZA treatments lowered N-cadherin transcript levels in MG-63 cells by ∼0.54 ($p < 0.001$) and 0.7 ($p < 0.001$) folds, respectively (Figure 4A). The immunoblot analysis supported the transcriptional findings confirming "cadherin-switching" by showing ∼0.3 ($p < 0.05$) and 0.5 ($p < 0.01$) folds increase in E-cadherin protein expression, compared to control, after PTER-ITC and ZA treatments, respectively. Similarly, PTER-ITC and ZA treatments reduced the N-cadherin expressions by ∼0.4 ($p < 0.05$) and 0.6 ($p < 0.01$) folds, respectively, in the MG-63 cells (Figure 4C).

Cytochrome c is released when the mitochondrial membrane potential is reduced, which activates Caspase-3 and leads to apoptosis.[42] As an intracellular protease, Caspase-3 plays an important role in the early stages of apoptosis. Activating Caspase-3 causes PARP cleavage, resulting in excessive ATP and $NAD^+$ consumption by the catalytic receptor process, ultimately leading to cell death.[43] In comparison to the control, the Caspase-3 mRNA levels were increased by ∼0.35 ($p < 0.01$) and 0.68 ($p < 0.001$) folds, respectively, with PTER-ITC and ZA treatments (Figure 4A). This effect was also marked at the protein level (Figure 4B) with almost 0.6 ($p < 0.01$) and 0.9 ($p < 0.001$) folds increase relative to control with PTER-ITC and ZA treatments, respectively (Figure 4C). Similarly, PARP-1 mRNA expression was also increased by 0.43 ($p < 0.001$) and 0.64 ($p < 0.001$)


https://doi.org/10.1021/acsomega.3c02732
ACS Omega 2023, 8, 43474−43489

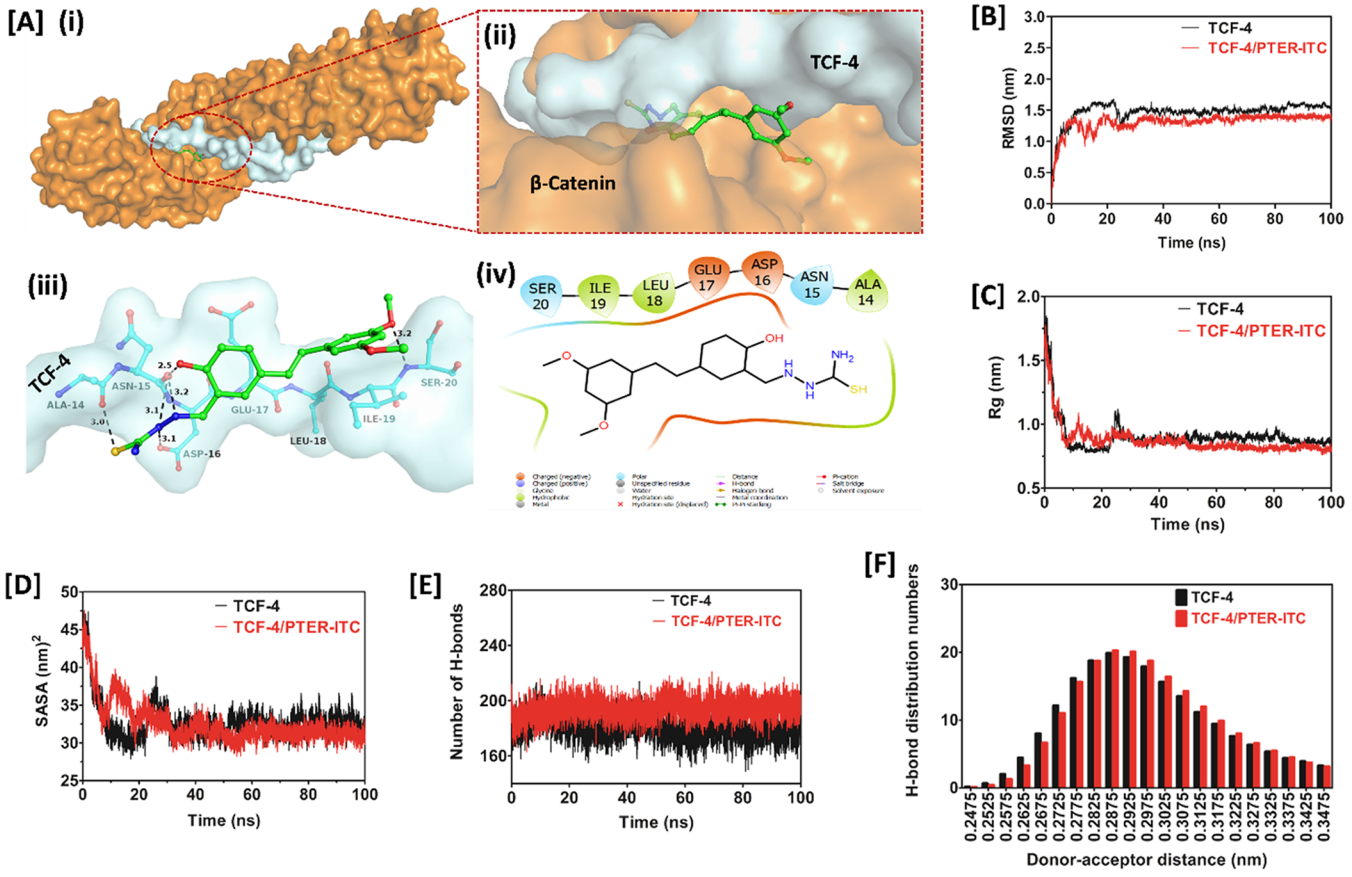


**Figure 5.** PTER-ITC inhibits $\beta$-catenin/TCF-4 interaction. (A) (i) Bird eye view of PTER-ITC interaction within $\beta$-catenin/TCF-4 complex; (ii) zoomed surface image of interacting PTER-ITC within $\beta$-catenin/TCF-4 complex; (iii) illustrative representation of PyMOL figure depicting the interactions at molecular level between PTER-ITC (green stick) and TCF-4 (cyan) within 4 Å (hydrogen bonded interactions are shown as black dotted lines); (iv) Maestro figure indicating the interacting residue of TCF-4 with PTER-ITC shown in green (hydrophobic), red (negatively charged), and cyan (polar). (B) RMSD of the backbone of TCF-4 (black) and TCF-4/PTER-ITC complex (red) from the 100 ns MD simulations. (C) $R_g$ profile of TCF-4 (black) and the TCF-4/PTER-ITC complex (red) from a 100 ns molecular simulation at 300 K. (D) SASA profile of TCF-4 (black) and TCF-4/PTER-ITC complex (red) for molecular simulation of 100 ns at 300 K. (E, F) Intraprotein hydrogen bond numbers (E) and intraprotein hydrogen bond distributions (F) during a 100 ns simulation at 300 K. Each experiment was repeated three times.

folds in response to PTER-ITC and ZA treatments, respectively, relative to control cells (Figure 4A). This change was also evident at the protein level (Figure 4B), which demonstrated an increase in cleaved PARP-1 protein of ~0.4 ($p < 0.05$) and 0.6 ($p < 0.01$) folds, respectively, following PTER-ITC and ZA treatments in comparison to control (Figure 4C). These findings collectively demonstrated that PTER-ITC effects, such as that of ZA, had an impact at both the transcriptional and translation levels.

Aberrant Wnt/$\beta$-catenin signaling through TCF-4 dependent transcriptional regulation plays a significant role in the pathophysiological manifestation of in many cancers, including osteosarcoma.[44,45] The variety of downstream processes, including cell−cell adhesion and apoptosis, are affected due to this altered signaling.[44] We observed that PTER-ITC treatment selectively affected osteosarcoma cells by reducing proliferation (evident from reduced PCNA expression), inducing apoptosis (evident from increased Caspase-3 and PARP-1 levels), and rescuing them from cadherin switching (increased E-cadherin levels while reducing N-cadherin) and EMT (evident from reduced levels of MMP-2 and MMP-9). Transcriptional regulators, Snail and Twist are known targets of TCF-4-mediated Wnt/$\beta$-catenin signaling,[46−48] which in turn further at the downstream level regulate E-cadherin, N-cadherin, MMP-2, MMP-9 and PCNA, among several other targets.[48−53] Additionally, in the etiology of many cancers, the feedforward loop established by the crosstalk between mitochondria and Wnt signaling is very crucial.[54,55] Based on our observation that PTER-ITC moderated the mitochondrial membrane potential in MG-63 osteosarcoma cells together with other related data helped us to trace back our way upstream from downstream target genes as Wnt signaling being a potential effector in this case.

**3.5. PTER-ITC Prevents TCF-4 Activation by Hindering Its Interaction with $\beta$-Catenin.** $\beta$-Catenin is a central key component of the Wnt signaling pathway, and aberrant expression or prolonged activation of $\beta$-catenin is frequently associated with cancer.[16] When $\beta$-catenin is translocated from the cytosol to the nucleus, it binds with TCF-4, to transcribe target genes such as cyclin D1 and c-myc. These genes significantly affect cell proliferation, migration, and survival. The osteosarcoma cells' ability to behave malignantly could be suppressed by inhibitors that target the $\beta$-catenin/TCF-4 interaction. Therefore, we investigated the possibility of PTER-ITC hampering this interaction by using molecular docking and molecular dynamic simulation.

Through molecular docking and dynamics, the interactions between PTER-ITC and TCF-4 was evaluated. With a free


https://doi.org/10.1021/acsomega.3c02732
ACS Omega 2023, 8, 43474−43489

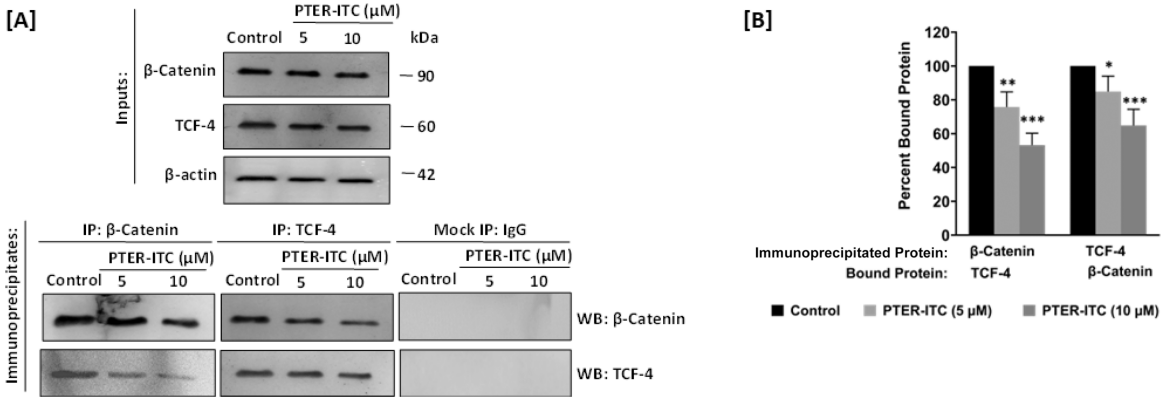


**Figure 6.** Biochemical validation of *in silico* data through Co-IP. (A) Representative immunoblots depicting the effect of PTER-ITC treatment on physical interaction between TCF-4 and *β*-catenin. (B) Bar graph depicting the densitometric analysis of (A) quantitatively demonstrating the effect of PTER-ITC treatment on the physical interaction between TCF-4 and *β*-catenin. Data represented as mean ± SE of three independent experiments. Statistical significance was determined through two-way ANOVA and represented as *, **, and *** for $p < 0.05$, 0.01, and 0.001, respectively, when compared to the respective control.

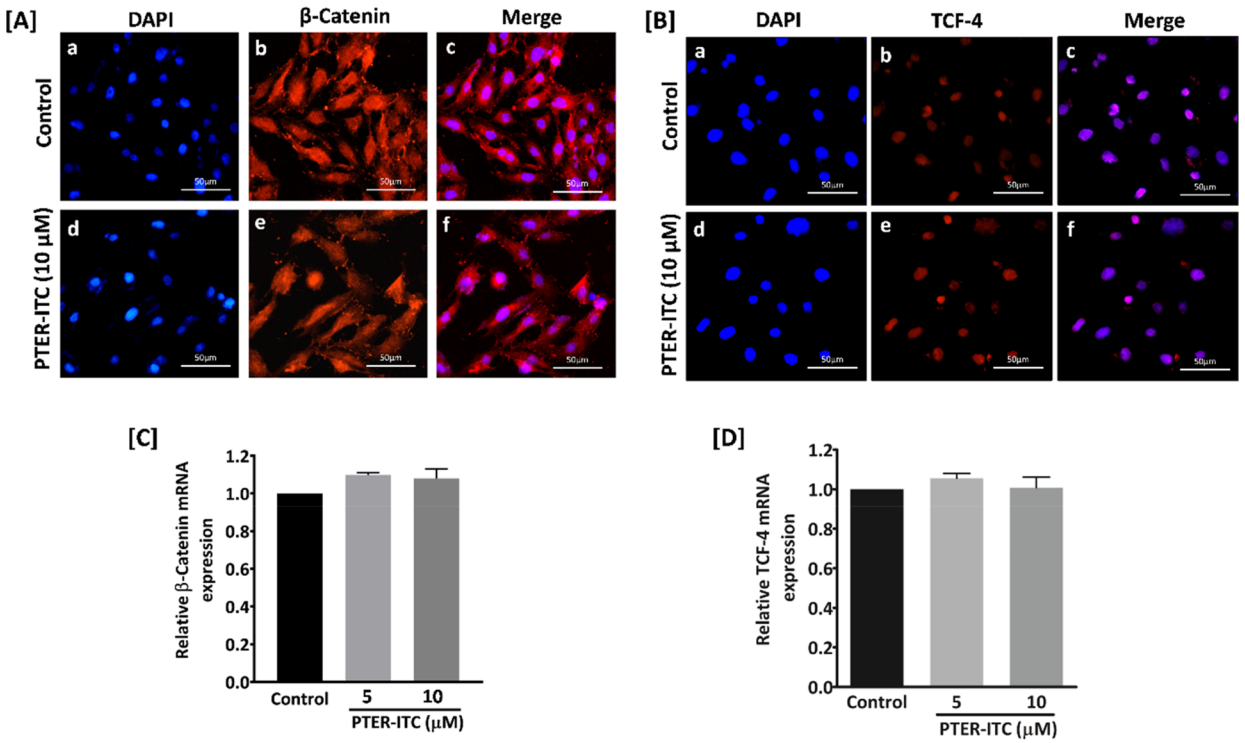


**Figure 7.** Effect of PTER-ITC on *β*-catenin and TCF-4 expression. (A, B) Representative immunofluorescent micrographs showing the effect of PTER-ITC treatment on (A) *β*-catenin and (B) TCF-4 protein expressions and their corresponding cellular localizations. (C, D) Bar graphs showing the effect of PTER-ITC treatment on (C) *β*-catenin and (D) TCF-4 mRNA expressions determined by RT-qPCR. Data are represented as mean ± SE of three independent experiments. All the experiments were repeated three times. Scale bar: 50 *μ*m.

energy change of −4.9 kcal mol$^{-1}$, PTER-ITC demonstrated binding at the *β*-catenin-interacting site of TCF-4. The interaction position of the best conformation is shown in Figure 5A [i (bird eye view), ii (zoomed surface view), and iii (interacting residue with PTER-ITC)]. According to the optimal binding conformation analysis, residues Ala14, Asn15, Asp16, Glu17, Leu 18, Ile19, and Ser20 were each involved in a unique interaction that contributed to the complex binding. PTER-ITC became stable in the active site of TCF-4 by forming five conventional hydrogen bonds with residues Ala14, Asn15, Asp16, and Ser20. Glu17 and Ile19 formed *π*-sigma bonds, while Asp 16 collaborated with TCF-4 to construct a salt bridge [Figure 5A, (iv)]. To further explore the stability and dynamic behavior of TCF-4 upon PTER-ITC binding, an MD simulation was conducted. The RMSD values of the TCF-4 backbone atoms were monitored to assess the stability. The RMSD of TCF-4 and PTER-ITC/TCF-4 complex remained constant at 1.5 and 1.3 nm, respectively, at 40 ns, as shown in Figure 5B. To demonstrate the compactness of protein and protein−ligand complexes, $R_g$ was computed. Indicating that the binding of PTER-ITC to TCF-4 resulted in the development of a stable complex, the PTER-ITC/TCF-4 complex has a lower mean $R_g$ value (0.81 nm) than TCF-4 protein (0.90 nm) alone (Figure 5C). Additionally, the SASA


https://doi.org/10.1021/acsomega.3c02732
ACS Omega 2023, 8, 43474−43489

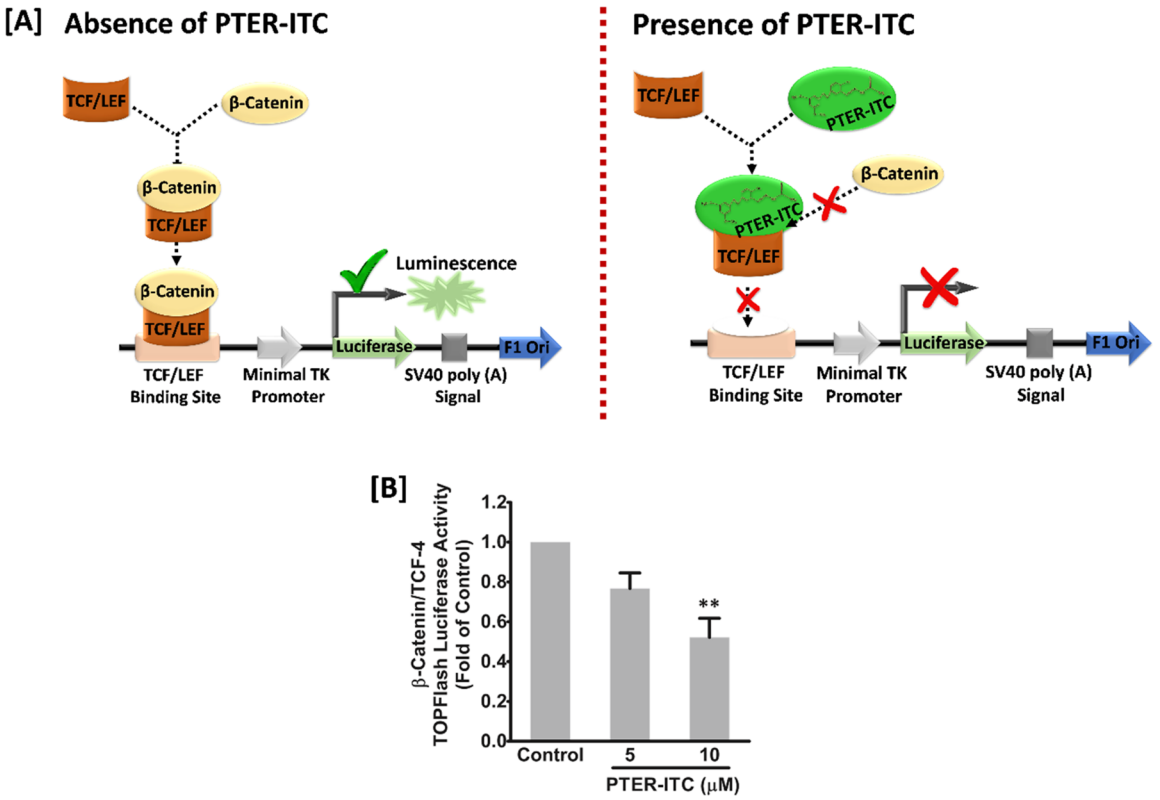


**Figure 8.** PTER-ITC inhibits transcriptional activation of TCF-4. (A) Schematic depiction of the principle behind the M50 Super 8x TOPFlash reporter assay. (B) Bar graph showing the effect of PTER-ITC treatment on $\beta$-catenin-mediated TCF-4 activity as fold change in luciferase activity over control. Data represented as mean ± SE of three independent experiments. Statistical significance of the observation was determined through one-way ANOVA and indicated as ** for $p < 0.01$ when compared to the control group.

profile revealed that the PTER-ITC/TCF-4 complex is more compact and stable (32.13 $nm^2$) than the TCF-4 protein (34.16 $nm^2$) alone (Figure 5D). PTER-ITC/TCF-4 contains a greater number of hydrogen bonds (194) than TCF-4 (180) alone, according to the intramolecular hydrogen-bonding map (Figure 5E). Hydrogen bond number distributions in only TCF-4 and PTER-ITC/TCF-4 complex revealed that both exhibit an affinity for hydrogen bonds between 0.255 to 0.34 nm (Figure 5F).

The results of the hydrogen bonding suggested that TCF-4 was in a stable conformation following PTER-ITC binding. The computational observation was biochemically validated through co-immunoprecipitation experiment (Figure 6A). For this experiment, TCF-4 was immunoprecipitated with an anti-$\beta$-catenin antibody from untreated cells. However, it was found that PTER-ITC treatments reduced the $\beta$-catenin-bound TCF-4 protein interaction, and this reduction was dose-dependent, as was evident from approximately 10−20 and 40−50% reductions in TCF-4/$\beta$-catenin interactions in the presence of 5 and 10 $\mu$M PTER-ITC, respectively (Figure 6B). In contrast, less TCF-4-bound $\beta$-catenin was found in a reverse co-immunoprecipitation setup compared to the untreated control. The input in the western blot analysis showed that PTER-ITC treatment did not affect the expression of $\beta$-catenin or TCF-4 (Figure 6). This was further validated through immunofluorescence and RT-qPCR analyses for $\beta$-catenin and TCF-4 (Figure 7A−D). The immunofluorescence expression of $\beta$-catenin demonstrated that PTER-ITC treatment had no impact on the protein's subcellular localization and nuclear translocation, as shown in Figure 7A. Additionally, it was observed that PTER-ITC did not alter the expression of TCF-4, which is located in the nucleus, even when it was present at the same level as that of untreated control cells using an immunofluorescence-based experimental approach similar to that with TCF-4 antibody (Figure 7B). Likewise, PTER-ITC had no impact on the mRNA expression levels of $\beta$-catenin and TCF-4 (Figure 7C and D). Taken together, these data demonstrated that PTER-ITC did not have any role in the expression and localization of both $\beta$-catenin and TCF-4, but it had a significant role in inhibiting their interactions.

A speculative model of the potential mechanism behind the transcription-regulatory activity of PTER-ITC was proposed based on the *in silico* and biochemical data and is depicted in Figure 8A. This hypothesis was then validated using the M50 Super 8X TOPFlash luciferase reporter assay. The luciferase reporter gene is located within this construct's TCF/lymphoid enhancer factor (LEF) regulatable promoter. TCF/LEF cannot bind to this promoter independently but only as a complex with $\beta$-catenin. As can be seen from Figure 8B, the transcription activator complex forms in the absence of PTER-ITC due to unhindered interaction between $\beta$-catenin and TCF-4, which activates the production of the luciferase reporter as indicated by increased luciferase activity in control cells. The formation of the transcription activator complex, which can bind to the promoter region of the luciferase construct, is suppressed in the presence of PTER-ITC, which results in a lower level of luciferase expression. It was found that the PTER-ITC dose was a factor behind the influence of luciferase expression. Although the observed reduction in luciferase expression at 5 $\mu$M PTER-ITC was not statistically


https://doi.org/10.1021/acsomega.3c02732
ACS Omega 2023, 8, 43474−43489

significant, half of the expression was reduced ($p < 0.01$) when the PTER-ITC dose was increased to 10 $\mu$M (Figure 8B). Due to PTER-ITC's interaction with TCF-4, as demonstrated in the structural analysis in the preceding section, the decrease in the luciferase activity further supported the finding that $\beta$-catenin and TCF-4 fail to interact with each other. The molecular understanding gained from the analysis of all of the data indicates that PTER-ITC inhibits the transcription of target genes that are activated by the $\beta$-catenin/TCF-4 complex combination.

## 4. DISCUSSIONS

As the most common type of primary bone cancer, osteosarcoma tends to affect more men than women, with most cases occurring after the age of 60 years.[56] The current work showed that PTER-ITC, a semi-synthetic compound, could inhibit cell proliferation and migration, decrease mitochondrial membrane potential, and induce apoptosis in osteosarcoma cells. Additionally, PTER-ITC promoted "cadherin-switching" by upregulating the expression of epithelial markers and downregulating the mesenchymal marker in osteosarcoma cells, thus reversing epithelial-mesenchymal transition (EMT). PTER-ITC attributes its anticancer effects in osteosarcoma cells by targeting the $\beta$-catenin/TCF-4 interaction in the Wnt/$\beta$-catenin signaling pathway.

We showed that PTER-ITC had an antiproliferative effect and efficiently reduced the metastatic potential of MG-63 cells using several cell-based assays. A proliferation marker, PCNA, was believed to be an auxiliary protein for DNA polymerases $\delta$ and $\varepsilon$ and therefore plays a role in DNA replication and repair. However, it was discovered to be involved in the cell cycle and apoptosis.[57] PCNA expression is a reliable indicator of the proliferative activity in various human neoplasia and is also overexpressed in osteosarcoma.[58] For this, PCNA was used in this study as a valid indicator of PTER-ITC's anticancer effect against MG-63 osteosarcoma cells. Our results, which align with earlier investigations, demonstrated that PTER-ITC had an antiproliferative effect on osteosarcoma cells by reducing PCNA levels.[59] Apoptosis is inextricably linked to changes in the mitochondrial membrane potential. Caspase-3 is activated by decreased mitochondrial membrane potential and releases cytochrome c.[40,42] Caspase-3 is a catalytic enzyme that cleaves PARP in a process that ATP and $NAD^+$ catalyzed and ultimately results in cell death.[43] The interplay between Wnt signaling and mitochondrial integrity is essential for cancer pathogenesis.[54,55] The moderation of the mitochondrial membrane potential by PTER-ITC suggested that Wnt signaling might be a possible target in this case. It is a well-known fact that in the case of osteosarcoma, the Wnt canonical pathway is constitutively activated, leading to aberrant stimulation of TCF-4/LEF transcriptional complex by $\beta$-catenin.[56] Wnt/$\beta$-catenin signaling includes two receptors: frizzled and LRP5/6 (low-density lipoprotein receptor-related protein), to which the Wnt ligand binds. The ligand binding to either of these receptors results in the deactivation of the $\beta$-catenin destruction complex, which consists of adenomatous polyposis coli (APC), axin, diversion, casein kinase I, and glycogen synthase kinase-3$\beta$ (GSK-3$\beta$), thus protecting $\beta$-catenin from its constitutive proteasomal degradation.[60] Free $\beta$-catenin accumulates in the cytoplasm and translocates into the nucleus, where it interacts with TCF-4 to form the transcription factor complex TCF/LEF, which then affects the expression of downstream target genes, such as cyclin D1 and c-myc. These genes maintain the primary tumorigenic traits like stemness, uncontrolled proliferation, and cancer cell survival.[61] Thus, the interaction of $\beta$-catenin and TCF-4 has the potential to be a very effective molecular target for new cancer therapies.

Although many Wnt signaling pathway inhibitors have been developed and all are still in the preclinical stage which can target the $\beta$-catenin/TCF-4 interaction.[62−64] For this reason, developing an inhibitor capable of binding to TCF-4 and subsequently inhibiting the $\beta$-catenin/TCF-4 interaction remains an unmet challenge. High selectivity for $\beta$-catenin/TCF-4 inhibitors is challenging to achieve since TCF-4 and APC/E-cadherin binding sites in $\beta$-catenin overlap with each other.[65] $\beta$-catenin and TCF-4 interaction facilitates cancer pathogenesis, but that with APC/E-cadherin requires normal cell functioning. Cell adhesion and normal stem cell functions depend on $\beta$-catenin's binding to E-cadherin, but its binding to APC is necessary for its degradation. Therefore, a new inhibitor that would selectively target the $\beta$-catenin/TCF-4 interaction and not interfere with the $\beta$-catenin/E-cadherin and $\beta$-catenin/APC interactions would be an ideal model. Consequently, this selective treatment approach will significantly improve the cytotoxicity against tumors. Drugs that specifically target the $\beta$-catenin/TCF-4 interaction will not harm normal cells at the same time.[66] By examining whether the semi-synthetic compound PTER-ITC could obstruct $\beta$-catenin/TCF-4 interaction by targeting the $\beta$-catenin-binding site in TCF-4, we attempted to address this challenging problem.

The current data confirmed that PTER-ITC could prevent $\beta$-catenin/TCF-4 interaction, thus inhibiting the downstream carcinogenic target genes. As it turns out, $\beta$-catenin interactions with E-cadherin or APC occur only in normal cells (Wnt Off state),[67−70] but constitutive $\beta$-catenin/TCF-4 interaction (Wnt On state) is a hallmark for several cancers.[71] Furthermore, molecular docking revealed that TCF-4/PTER-ITC (−4.9 kcal $mol^{-1}$) interactions (Figure 5A i-iv) are stronger than the interactions of E-cadherin/PTER-ITC (−3.1 kcal $mol^{-1}$), APC/PTER-ITC (−3.9 kcal $mol^{-1}$), and $\beta$-catenin/PTER-ITC (−4.1 kcal $mol^{-1}$) (Supplementary Figure S1A−C). Additionally, PTER-ITC engages the Asp16 residue in TCF-4, which is crucial for high affinity binding with $\beta$-catenin.[24] APC plays a significant role in cell proliferation.[72,73] Our observation that PTER-ITC is noncytotoxic to normal human osteoblastic hFOB 1.19 cells (Figure 1B) supports a weaker or potentially nonexistent interaction between APC and PTER-ITC. Our RT-qPCR and immunofluorescence results showed that PTER-ITC did not affect $\beta$-catenin or TCF-4 expressions *per se*. However, findings from molecular docking, molecular dynamic simulation, and co-immunoprecipitation revealed that PTER-ITC significantly and exclusively disrupted the interaction of $\beta$-catenin/TCF-4. Data from the MD simulation indicated that the interaction between TCF-4 and PTER-ITC is remarkably stable. Further evidence on binding of PTER-ITC to the active site of TCF-4 resulting in a stable complex is provided by the RMSD, $R_g$, SASA, and hydrogen bonding values from the molecular dynamics simulation data. Thus, the current biophysical data show that $\beta$-catenin fails to interact with the TCF-4/LEF complex in the presence of PTER-ITC. PTER-ITC inhibits the expression of downstream target genes responsible for tumorigenesis by occupying the $\beta$-catenin binding site in TCF-4. $\beta$-catenin and TCF-4 interact when the Wnt pathway is activated in the case


https://doi.org/10.1021/acsomega.3c02732
ACS Omega 2023, 8, 43474−43489

of cancer to promote its pathogenesis. Consequently, this prevents the interactions of β-catenin with E-cadherin and APC through a cascade of signaling events.[74] This aspect is extremely crucial since it allows any therapeutics to exert its effects on cancer cells only, sparing normal cells.

The present data also indicated the same when it was found that PTER-ITC could inhibit the migration and proliferation of osteosarcoma cells (MG-63 cells) but was almost ineffective toward the normal cells (hFOB 1.19 cells). Thus, it is likely that PTER-ITC can reduce the nonspecific side effects by making β-catenin available for interactions with APC and E-cadherin, which are required for normal cell physiology, through its binding to TCF-4.[65] This hypothesis has the corollary effect that if β-catenin is free to interact with E-cadherin in the presence of PTER-ITC, it would facilitate cell adhesion and promote the reversal of metastasis in osteosarcoma cells. The current study's wound-healing and transwell migration assays showed that PTER-ITC prevented osteosarcoma cells from migrating. MMPs are significant proteolytic enzymes that play important roles in the EMT process, migration, and invasion. During metastasis, they damage the extracellular matrix and basement membrane.[75] Osteosarcoma cells undergo EMT, a rare phenotypic transformation that carries invasive properties. Epithelial marker genes are inhibited during carcinoma metastasis, and this is accompanied by an increase in the mesenchymal markers, which is caused by EMT.[76] E-cadherin, a transmembrane glycoprotein, could regulate cell−cell adhesion. When cells undergo EMT, they exhibit a decreased expression of E-cadherin, while N-cadherin, a calcium-dependent adhesion molecule is increased that promotes tumor cell metastasis by resisting protease hydrolysis.[77] The present study distinctly showed that PTER-ITC could concurrently upregulate epithelial markers and downregulate mesenchymal markers in osteosarcoma cells.

This *in vitro* preliminary study reveals the potential of PTER-ITC as a promising therapeutic against osteosarcoma. Additional in-depth research using a xenograft mouse model and other osteosarcoma cell lines is required to make PTER-ITC a realistic therapy option for osteosarcoma. However, the data from the current study are sufficient to establish PTER-ITC as a leading antiosteosarcoma compound and support the need for further studies using improved *in vitro* and *in vivo* models to demonstrate the therapeutic efficacy and identify the precise mechanism(s) of action for this compound.

## 5. CONCLUSIONS

Despite considerable research, osteosarcoma persists as a formidable malignancy to cure, and survival rates for this aggressive bone cancer have not improved significantly in recent years. The lack of understanding of the causes of osteosarcoma has contributed to a standstill in research. To the best of our knowledge, the current study is the first ever report on the potent antiosteosarcoma properties of the hybrid molecule PTER-ITC. Naturally establishing such a compound for anticancer therapeutics especially for osteosarcoma, where the scope of its cure and management is very limited, this compound may in future play a critical role in bone related cancer. According to the above findings, the PTER-ITC conjugate significantly reduced the cell proliferation, induced apoptosis, disrupted mitochondrial membrane potential, and reversed EMT in osteosarcoma cells. The cytotoxicity data are quite promising because of two reasons: (i) PTER-ITC conjugate is significantly more effective than its parent compound PTER and (ii) it selectively targeted and induced apoptosis in osteosarcoma (MG-63) cells without any effect on the noncancerous hFOB 1.19 cells. Further, PTER-ITC targeted the β-catenin/TCF-4 interaction by occupying the β-catenin binding site of TCF-4 without interfering in their respective expressions. This was another advantage of this compound since both β-catenin and TCF-4 are known to have other functions in normal cells. Collectively, it can be concluded that the selectivity of PTER-ITC in targeting only osteosarcoma cells, as evident from the current cell culture based *in vitro* studies, is because of its potential to target the aberrant Wnt/β-catenin signaling in cancer cells only. Our findings therefore have identified PTER-ITC as a lead anticancer compound against osteosarcoma, which can selectively kill only cancer cells and is safe for normal cells, under *in vitro* conditions. All of these data present in this study warrant further systematic preclinical and pharmacological validations under *in vivo* conditions to appreciate its future health beneficial effect as a drug molecule for the cure and management of bone cancer.

## ■ ASSOCIATED CONTENT

### Supporting Information

The Supporting Information is available free of charge at https://pubs.acs.org/doi/10.1021/acsomega.3c02732.

Supplementary figure along with legend on Molecular Docking of PTER-ITC with adenomatous polyposis coli (APC), E-cadherin, and β-catenin showing PyMOL generated molecular docking representations of interactions of PTER-ITC with APC, E-cadherin, and β-catenin with respective binding energies (PDF)

## ■ AUTHOR INFORMATION


### Corresponding Author

**Partha Roy** − *Department of Biosciences and Bioengineering, Indian Institute of Technology Roorkee, Roorkee, Uttarakhand 247667, India;* orcid.org/0000-0003-1943-3079; Email: partha.roy@bt.iitr.ac.in

### Authors

**Viney Kumar** − *Department of Biosciences and Bioengineering, Indian Institute of Technology Roorkee, Roorkee, Uttarakhand 247667, India;* Present Address: Department of Pathology, Albert Einstein College of Medicine, New York, USA; orcid.org/0000-0003-3677-3489

**Swati Haldar** − *Department of Biosciences and Bioengineering, Indian Institute of Technology Roorkee, Roorkee, Uttarakhand 247667, India; Centre of Nanotechnology, Indian Institute of Technology Roorkee, Roorkee 247667 Uttarakhand, India;* Present Address: Department of Genetics, Albert Einstein College of Medicine, New York, USA.; orcid.org/0000-0002-1566-1907

**Souvik Ghosh** − *Department of Biosciences and Bioengineering, Indian Institute of Technology Roorkee, Roorkee, Uttarakhand 247667, India; Centre of Nanotechnology, Indian Institute of Technology Roorkee, Roorkee 247667 Uttarakhand, India;* orcid.org/0000-0002-6524-0887

**Saakshi Saini** − *Department of Biosciences and Bioengineering, Indian Institute of Technology Roorkee, Roorkee, Uttarakhand 247667, India*




https://doi.org/10.1021/acsomega.3c02732
ACS Omega 2023, 8, 43474−43489

**Poonam Dhankhar** − *Department of Biosciences and Bioengineering, Indian Institute of Technology Roorkee, Roorkee, Uttarakhand 247667, India;* Present Address: Department of Physiology and Biophysics, Weill Medical College of Cornell University, New York, USA.

Complete contact information is available at: https://pubs.acs.org/10.1021/acsomega.3c02732

### Funding

This work was supported by a research grant from the Department of Biotechnology, Government of India (Grant No. BT/PR12138/MED/97/238/2014) to PR.

### Notes

The authors declare no competing financial interest.

## ■ ACKNOWLEDGMENTS

The authors would like to convey their sincere thanks to Dr. Naibedya Chattopadhyay of CSIR-Central Drug Research Institute, Lucknow, India, for the kind gift of the hFOB 1.19 cell line. The authors would like to convey their sincere thanks to Council for Scientific and Industrial Research (CSIR), Government of India, for providing research fellowship [9/143(0897)/2017-EMR-I] to V.K. The authors would also like to thank NMRbox: National Center for Biomolecular NMR Data Processing and Analysis, a Biomedical Technology Research Resource (BTRR), which is supported by NIH grant no. P41GM111135 (NIGMS). The authors acknowledge the nonacademic and technical support from the departmental offices of the Department of Bioscience and Bioengineering and the Sponsored Research and Industrial Consultancy of Indian Institute of Technology Roorkee, India.

## ■ ABBREVIATIONS

AML, acute myeloid leukemia; ANOVA, analysis of variance; AO, acridine orange; APC, adenomatous polyposis coli; ATCC, American Type Culture Collection; BSA, bovine serum albumin; Co-IP, co-immunoprecipitation; DAPI, 4′,6-diamidino-2-phenylindole dihydrochloride; DMEM-F12, Dulbecco's modified Eagle's medium-F12; ECL, electrochemiluminescent; ECM, extracellular matrix; EMT, epithelial-mesenchymal transition; EtBr, ethidium bromide; FBS, fetal bovine serum; FDA, Food and Drug Administration; GROMACS, Groningen machine for chemical simulations; GSK-3$\beta$, glycogen synthase kinase-3$\beta$; $IC_{50}$, half-maximal inhibitory concentration; LEF, lymphoid enhancer factor; LGA, lamarckian genetic algorithm; MD, molecular dynamics; MDR, multidrug resistance; MMP-2, matrix metalloproteinase-2; MMP-9, matrix metalloproteinase-9; MTT, 3-[4,5-dimethylthiazol-2-yl]2,5-diphenyl tetrazolium bromide; NCCS, National Centre for Cell Science; nm, nanometer; NPT, number of particles, pressure, and temperature; ns, nanoseconds; NVT, number of particles, volume, and temperature; PARP-1, poly [ADP-ribose] polymerase-1; PCNA, proliferative cell nuclear antigen; ps, picosecond; PTER, pterostilbene; PTER-ITC, pterostilbene-isothiocyanate; $R_g$, radius of gyration; RMSD, root mean square deviation; SASA, solvent-accessible surface area; SE, standard error; SPC, simple point charges; TCF-4, transcription factor-4; TdT, terminal deoxynucleotidyl transferase; TUNEL, terminal deoxynucleotidyl transferase dUTP nick end labeling; UFF, universal force field; ZA, zoledronic acid; $\alpha$-MEM, minimal essential medium with alpha modification; $\mu$M, micromolar

## ■ REFERENCES

(1) Xu, Y.; Qi, J.; Sun, W.; Zhong, W.; Wu, H. Therapeutic Effects of Zoledronic Acid-Loaded Hyaluronic Acid/Polyethylene Glycol/Nano-Hydroxyapatite Nanoparticles on Osteosarcoma. *Front. Bioeng. Biotechnol.* **2022**, *10*, 1−14.

(2) Yu, S.; Fourman, M. S.; Mahjoub, A.; Mandell, J. B.; Crasto, J. A.; Greco, N. G.; Weiss, K. R. Lung Cells Support Osteosarcoma Cell Migration and Survival. *BMC Cancer* **2017**, *17* (1), 1−10.

(3) Zhang, N.; Ying, M. D.; Wu, Y. P.; Zhou, Z. H.; Ye, Z. M.; Li, H.; Lin, D. S. Hyperoside, a Flavonoid Compound, Inhibits Proliferation and Stimulates Osteogenic Differentiation of Human Osteosarcoma Cells. *PLoS One* **2014**, *9* (7), e98973.

(4) Siegel, R.; Naishadham, D.; Jemal, A. Cancer Statistics, 2013. *CA. Cancer J. Clin.* **2013**, *63* (1), 11−30.

(5) Tran, T. H.; Ramasamy, T.; Choi, J. Y.; Nguyen, H. T.; Pham, T. T.; Jeong, J.-H.; Ku, S. K.; Choi, H.-G.; Yong, C. S.; Kim, J. O. Tumor-Targeting, PH-Sensitive Nanoparticles for Docetaxel Delivery to Drug-Resistant Cancer Cells. *Int. J. Nanomedicine* **2015**, *10* (1), 5249−5262.

(6) Thorn, C. F.; Oshiro, C.; Marsh, S.; Hernandez-Boussard, T.; McLeod, H.; Klein, T. E.; Altman, R. B. Doxorubicin Pathways: Pharmacodynamics and Adverse Effects. *Pharmacogenet. Genomics* **2011**, *21* (7), 440−446.

(7) Hernández, Á. P.; Díez, P.; García, P. A.; Miguel Del Corral, J. M.; Pérez-Andrés, M.; Díez, D.; San Feliciano, A.; Fuentes, M.; Castro, M. Á. New Hybrids Derived from Podophyllic Aldehyde and Diterpenylhydroquinones with Selectivity toward Osteosarcoma Cells. *ACS Med. Chem. Lett.* **2018**, *9* (4), 328−333.

(8) Newman, D. J.; Cragg, G. M. Natural Products as Sources of New Drugs from 1981 to 2014. *J. Nat. Prod.* **2016**, *79* (3), 629−661.

(9) Decker, M. Hybrid Molecules Incorporating Natural Products: Applications in Cancer Therapy, Neurodegenerative Disorders and Beyond. *Curr. Med. Chem.* **2011**, *18* (10), 1464−1475.

(10) Goyal, S.; Gupta, N.; Chatterjee, S.; Nimesh, S. Natural Plant Extracts as Potential Therapeutic Agents for the Treatment of Cancer. *Curr. Top. Med. Chem.* **2016**, *17* (2), 96−106.

(11) Nikhil, K.; Sharan, S.; Chakraborty, A.; Bodipati, N.; Krishna Peddinti, R.; Roy, P. Role of Isothiocyanate Conjugate of Pterostilbene on the Inhibition of MCF-7 Cell Proliferation and Tumor Growth in Ehrlich Ascitic Cell Induced Tumor Bearing Mice. *Exp. Cell Res.* **2014**, *320* (2), 311−328.

(12) Nikhil, K.; Sharan, S.; Roy, P. A Pterostilbene Derivative Suppresses Osteoclastogenesis by Regulating RANKL-Mediated NF-KB and MAPK Signalling in RAW264.7 Cells. *Pharmacol. Reports* **2015**, *67*, 1264−1272.

(13) Nikhil, K.; Sharan, S.; Chakraborty, A.; Roy, P. Pterostilbene-Isothiocyanate Conjugate Suppresses Growth of Prostate Cancer Cells Irrespective of Androgen Receptor Status. *PLoS One* **2014**, *9* (4), e93335.

(14) Nikhil, K.; Sharan, S.; Palla, S. R.; Sondhi, S. M.; Peddinti, R. K.; Roy, P. Understanding the Mode of Action of a Pterostilbene Derivative as Anti-Inflammatory Agent. *Int. Immunopharmacol.* **2015**, *28* (1), 10−21.

(15) Kumar, V.; Haldar, S.; Das, N. S.; Ghosh, S.; Dhankhar, P.; Sircar, D.; Roy, P. Pterostilbene-Isothiocyanate Inhibits Breast Cancer Metastasis by Selectively Blocking IKK-$\beta$/NEMO Interaction in Cancer Cells. *Biochem. Pharmacol.* **2021**, *192*, No. 114717.

(16) Shin, S. H.; Lim, D. Y.; Reddy, K.; Malakhova, M.; Liu, F.; Wang, T.; Song, M.; Chen, H.; Bae, K. B.; Ryu, J.; Liu, K.; Lee, M. H.; Bode, A. M.; Dong, Z. A Small Molecule Inhibitor of the $\beta$-Catenin-TCF4 Interaction Suppresses Colorectal Cancer Growth In Vitro and In Vivo. *EBioMedicine* **2017**, *25*, 22−31.

(17) Yi, T.; Cho, S.; Yi, Z.; Pang, X.; Rodriguez, M.; Wang, Y.; Sethi, G.; Aggarwal, B. B.; Liu, M. Thymoquinone Inhibits Tumor Angiogenesis and Tumor Growth through Suppressing AKT and ERK Signaling Pathways. *Mol. Cancer Ther.* **2008**, *7* (7), 1789−1796.

(18) Silva Nunes, J. P.; Martins Dias, A. A. ImageJ Macros for the User-Friendly Analysis of Soft-Agar and Wound-Healing Assays. *Biotechniques* **2017**, *62* (4), 175−179.

(19) Justus, C. R.; Leffler, N.; Ruiz-Echevarria, M.; Yang, L. V. In Vitro Cell Migration and Invasion Assays. *J. Vis. Exp.* **2014**, *88*, 1−8.
(20) Schneider, C. A.; Rasband, W. S.; Eliceiri, K. W. NIH Image to ImageJ: 25 Years of Image Analysis. *Nat. Methods* **2012**, *9* (7), 671−675.
(21) Graham, T. A.; Ferkey, D. M.; Mao, F.; Kimelman, D.; Xu, W. Tcf4 Can Specifically Recognize β-Catenin Using Alternative Conformations. *Nat. Struct. Biol.* **2001**, *8* (12), 1048−1052.
(22) Morris, G. M.; Huey, R.; Lindstrom, W.; Sanner, M. F.; Belew, R. K.; Goodsell, D. S.; Olson, A. J. AutoDock4 and AutoDockTools4: Automated Docking with Selective Receptor Flexibility. *J. Comput. Chem.* **2009**, *30* (16), 2785−2791.
(23) O'Boyle, N. M.; Banck, M.; James, C. A.; Morley, C.; Vandermeersch, T.; Hutchison, G. R. Open Babel : An Open Chemical Toolbox. *J. Cheminform.* **2011**, *3* (33), 1−14.
(24) Poy, F.; Lepourcelet, M.; Shivdasani, R. A.; Eck, M. J. Structure of a Human Tcf4-β-Catenin Complex. *Nat. Struct. Biol.* **2001**, *8* (12), 1053−1057.
(25) DeLano, W. L. Pymol: An Open-Source Molecular Graphics Tool. *CCP4 Newsl. Protein Crystallogr.* **2002**, *40*, 82−92.
(26) Maciejewski, M. W.; Schuyler, A. D.; Gryk, M. R.; Moraru, I. I.; Romero, P. R.; Ulrich, E. L.; Eghbalnia, H. R.; Livny, M.; Delaglio, F.; Hoch, J. C. NMRbox: A Resource for Biomolecular NMR Computation. *Biophys. J.* **2017**, *112* (8), 1529−1534.
(27) van Gunsteren, W. F. *Biomolecular Simulation: The GROMOS96 Manual and User Guide*; Hochschulverlag AG an der ETH Zürich: Zürich, 1996.
(28) Van Der Spoel, D.; Lindahl, E.; Hess, B.; Groenhof, G.; Mark, A. E.; Berendsen, H. J. C. GROMACS: Fast, Flexible, and Free. *J. Comput. Chem.* **2005**, *26* (16), 1701−1718.
(29) Schüttelkopf, A. W.; Van Aalten, D. M. F. PRODRG: A Tool for High-Throughput Crystallography of Protein-Ligand Complexes. *Acta Crystallogr. Sect. D Biol. Crystallogr.* **2004**, *60* (8), 1355−1363.
(30) Singh, N.; Dalal, V.; Kumar, P. Structure Based Mimicking of Phthalic Acid Esters (PAEs) and Inhibition of HACMSD, an Important Enzyme of the Tryptophan Kynurenine Metabolism Pathway. *Int. J. Biol. Macromol.* **2018**, *108*, 214−224.
(31) Dhankhar, P.; Dalal, V.; Singh, V.; Tomar, S.; Kumar, P. Computational Guided Identification of Novel Potent Inhibitors of N-Terminal Domain of Nucleocapsid Protein of Severe Acute Respiratory Syndrome Coronavirus 2. *J. Biomol. Struct. Dyn.* **2022**, *40*, 4084−4099.
(32) Berendsen, H. J. C.; Postma, J. P. M.; Van Gunsteren, W. F.; Dinola, A.; Haak, J. R. Molecular Dynamics with Coupling to an External Bath. *J. Chem. Phys.* **1984**, *81* (8), 3684−3690.
(33) Parrinello, M.; Rahman, A. Polymorphic Transitions in Single Crystals: A New Molecular Dynamics Method. *J. Appl. Phys.* **1981**, *52* (12), 7182−7190.
(34) Veeman, M. T.; Slusarski, D. C.; Kaykas, A.; Louie, S. H.; Moon, R. T. Zebrafish Prickle, a Modulator of Noncanonical Wnt/Fz Signaling, Regulates Gastrulation Movements. *Curr. Biol.* **2003**, *13* (8), 680−685.
(35) Ory, B.; Blanchard, F.; Battaglia, S.; Gouin, F.; Rédini, F.; Heymann, D. Zoledronic Acid Activates the DNA S-Phase Checkpoint and Induces Osteosarcoma Cell Death Characterized by Apoptosis-Inducing Factor and Endonuclease-G Translocation Independently of P53 and Retinoblastoma Status. *Mol. Pharmacol.* **2007**, *71* (1), 333−343.
(36) Sun, Y.; Liu, L.; Wang, Y.; He, A.; Hu, H.; Zhang, J.; Han, M.; Huang, Y. Curcumin Inhibits the Proliferation and Invasion of MG-63 Cells through Inactivation of the p-JAK2/ p-STAT3 Pathway. *Onco. Targets. Ther.* **2019**, *12*, 2011−2021.
(37) Loh, C. Y.; Chai, J. Y.; Tang, T. F.; Wong, W. F.; Sethi, G.; Shanmugam, M. K.; Chong, P. P.; Looi, C. Y. The E-Cadherin and N-Cadherin Switch in Epithelial-to-Mesenchymal Transition: Signaling, Therapeutic Implications, and Challenges. *cells* **2019**, *8* (10), 1118.
(38) Schech, A. J.; Kazi, A. A.; Gilani, R. A.; Brodie, A. H. Zoledronic Acid Reverses the Epithelial − Mesenchymal Transition and Inhibits Self-Renewal of Breast Cancer Cells through Inactivation of NF- k B. *Mol. Cancer Ther.* **2013**, *12* (7), 1356−1367.
(39) Zhao, X.; Zhang, Q.; Chen, L. Triptolide Induces the Cell Apoptosis of Osteosarcoma Cells through the TRAIL Pathway. *Oncol. Rep.* **2016**, *36*, 1499−1505.
(40) Goldar, S.; Khaniani, M. S.; Derakhshan, S. M.; Baradaran, B. Molecular Mechanisms of Apoptosis and Roles in Cancer Development and Treatment. *Asian Pacific J. Cancer Prev.* **2015**, *16* (6), 2129−2144.
(41) Cabral-Pacheco, G. A; Garza-Veloz, I.; Castruita-De la Rosa, C.; Ramirez-Acuna, J. M; Perez-Romero, B. A; Guerrero-Rodriguez, J. F; Martinez-Avila, N.; Martinez-Fierro, M. L The Roles of Matrix Metalloproteinases and Their Inhibitors in Human Diseases. *Int. J. Mol. Sci.* **2020**, *21*, 9739.
(42) Garrido, C.; Galluzzi, L.; Brunet, M.; Puig, P. E.; Didelot, C.; Kroemer, G. Mechanisms of Cytochrome c Release from Mitochondria. *Cell Death Differ.* **2006**, *13* (9), 1423−1433.
(43) Kuzhandaivel, A.; Nistri, A.; Mladinic, M. Kainate-Mediated Excitotoxicity Induces Neuronal Death in the Rat Spinal Cord in Vitro via a PARP-1 Dependent Cell Death Pathway (Parthanatos). *Cell. Mol. Neurobiol.* **2010**, *30* (7), 1001−1012.
(44) Chen, C.; Zhao, M.; Tian, A.; Zhang, X.; Yao, Z.; Ma, X. Aberrant Activation of Wnt/β-Catenin Proliferation of Bone Sarcoma Cells Signaling Drives. *Oncotarget* **2015**, *6* (19), 17570−17583.
(45) Bian, J.; Dannappel, M.; Wan, C.; Firestein, R. Transcriptional Regulation of Wnt/β -Catenin Pathway in Colorectal Cancer. *Cells* **2020**, *9*, 2125.
(46) Howe, L. R.; Watanabe, O.; Leonard, J.; Brown, A. M. C. Twist Is Up-Regulated in Response to Wnt1 and Inhibits Mouse Mammary Cell Differentiation. *Cancer Res.* **2003**, *63* (8), 1906−1913.
(47) ten Berge, D.; Koole, W.; Fuerer, C.; Fish, M.; Eroglu, E.; Nusse, R. Wnt Signaling Mediates Self-Organization and Axis Formation in Embryoid Bodies. *Cell Stem Cell* **2008**, *3* (5), 508−518.
(48) Luo, G.; Li, J.; Wen, J.; Zhou, Y.; Hu, Y.; Zhou, J. Effect and Mechanism of the Twist Gene on Invasion and Metastasis of Gastric Carcinoma Cells. *World J. Gastroenterol.* **2008**, *14* (16), 2487−2493.
(49) Medici, D.; Hay, E. D.; Olsen, B. R. Snail and Slug Promote Epithelial-Mesenchymal Transition through Beta-Catenin − T-Cell Factor-4-Dependent Expression of Transforming Growth Factor- Beta 3. *Mol. Biol. C* **2008**, *19*, 4875−4887.
(50) Miyoshi, A.; Kitajima, Y.; Kido, S.; Shimonishi, T.; Matsuyama, S.; Kitahara, K.; Miyazaki, K. Snail Accelerates Cancer Invasion by Upregulating MMP Expression and Is Associated with Poor Prognosis of Hepatocellular Carcinoma. *Br. J. Cancer* **2005**, *92*, 252−258.
(51) Wu, W.; You, R.; Cheng, C.; Lee, M.; Lin, T.; Hu, C. Snail Collaborates with EGR-1 and SP-1 to Directly Activate Transcription of MMP 9 and ZEB1. *Sci. Reports* **2017**, *7*, 17753.
(52) Park, J. H.; Sung, I. J.; Lee, S. W.; Kim, K. W.; Kim, Y. S.; Yoo, M. A. The Zinc-Finger Transcription Factor Snail Downregulates Proliferating Cell Nuclear Antigen Expression in Colorectal Carcinoma Cells. *Int. J. Oncol.* **2005**, *26* (6), 1541−1547.
(53) Xu, Y.; Qin, L.; Sun, T.; Wu, H.; He, T.; Yang, Z.; Mo, Q.; Liao, L.; Xu, J. Twist1 Promotes Breast Cancer Invasion and Metastasis by Silencing Foxa1 Expression. *Oncogene* **2017**, *36* (8), 1157−1166.
(54) Delgado-Deida, Y.; Alula, K. M.; Theiss, A. L. The Influence of Mitochondrial-Directed Regulation of Wnt Signaling on Tumorigenesis. *Gastroenterol. Rep.* **2020**, *8* (3), 215−223.
(55) Brown, K.; Yang, P.; Salvador, D.; Kulikauskas, R.; Ruohola-Baker, H.; Robitaille, A. M.; Chien, A. J.; Moon, R. T.; Sherwood, V. WNT/β-Catenin Signaling Regulates Mitochondrial Activity to Alter the Oncogenic Potential of Melanoma in a PTEN-Dependent Manner. *Oncogene* **2017**, *36*, 3119−3136.
(56) Lin, C. H.; Ji, T.; Chen, C. F.; Hoang, B. H. Wnt Signaling in Osteosarcoma. *Adv. Exp. Med. Biol.* **2014**, *804*, 33−45.
(57) Choe, K. N.; Moldovan, G. L. Forging Ahead through Darkness: PCNA, Still the Principal Conductor at the Replication Fork. *Mol. Cell* **2017**, *65* (3), 380−392.


https://doi.org/10.1021/acsomega.3c02732
*ACS Omega* 2023, 8, 43474−43489

(58) Park, H. R.; Park, Y. K. Expression of P53 Protein, PCNA, and Ki-67 in Osteosarcomas of Bone. *J. Korean Med. Sci.* **1995**, *10*, 360−367.
(59) Wang, X.; Wang, D.; Yuan, N.; Liu, F.; Wang, F.; Wang, B.; Zhou, D. The Prognostic Value of PCNA Expression in Patients with Osteosarcoma: A Meta-Analysis of 16 Studies. *Medicine (Baltimore).* **2017**, *96* (41), No. e8254.
(60) Gumbiner, B. M. Carcinogenesis: A Balance between β-Catenin and APC. *Curr. Biol.* **1997**, *7* (7), 443−446.
(61) Shang, S.; Hua, F.; Hu, Z. W. The Regulation of β-Catenin Activity and Function in Cancer: Therapeutic Opportunities. *Oncotarget* **2017**, *8* (20), 33972−33989.
(62) Yan, M.; Li, G.; An, J. Discovery of Small Molecule Inhibitors of the Wnt/β-Catenin Signaling Pathway by Targeting β-Catenin/Tcf4 Interactions. *Exp. Biol. Med.* **2017**, *242* (11), 1185−1197.
(63) Catrow, J. L.; Zhang, Y.; Zhang, M.; Ji, H. Discovery of Selective Small-Molecule Inhibitors for the β-Catenin/T-Cell Factor Protein−Protein Interaction through the Optimization of the Acyl Hydrazone Moiety. *ACS Med. Chem.* **2015**, *58*, 4678−4692.
(64) Kahn, M. Can We Safely Target the WNT Pathway? *Nat. Rev. Drug Discovery* **2014**, *13* (7), 513−532.
(65) Cheng, X.; Xu, X.; Chen, D.; Zhao, F.; Wang, W. Therapeutic Potential of Targeting the Wnt/β-Catenin Signaling Pathway in Colorectal Cancer. *Biomed. Pharmacother.* **2019**, *110*, 473−481.
(66) Isakoff, M. S.; Bielack, S. S.; Meltzer, P.; Gorlick, R. Osteosarcoma: Current Treatment and a Collaborative Pathway to Success. *J. Clin. Oncol.* **2015**, *33* (27), 3029−3035.
(67) Centelles, J. J. General Aspects of Colorectal Cancer. *ISRN Oncol.* **2012**, *2012*, 1−19.
(68) Yu, W. K.; Xu, Z. Y.; Yuan, L.; Mo, S.; Xu, B.; Cheng, X. D.; Qin, J. J. Targeting β-Catenin Signaling by Natural Products for Cancer Prevention and Therapy. *Front. Pharmacol.* **2020**, *11*, 1−12.
(69) Zhang, Y.; Wang, X. Targeting the Wnt/β-Catenin Signaling Pathway in Cancer. *J. Hematol. Oncol.* **2020**, *13*, 165.
(70) Chae, W. J.; Bothwell, A. L. M. Canonical and Non-Canonical Wnt Signaling in Immune Cells. *Trends Immunol.* **2018**, *39* (10), 830−847.
(71) Sharma, A.; Mir, R.; Galande, S. Epigenetic Regulation of the Wnt/β-Catenin Signaling Pathway in Cancer. *Front. Genet.* **2021**, *12*, 1−27.
(72) Parisi, A.; Lacour, F.; Giordani, L.; Colnot, S.; Maire, P.; Le Grand, F. APC Is Required for Muscle Stem Cell Proliferation and Skeletal Muscle Tissue Repair. *J. Cell Biol.* **2015**, *210* (5), 717−726.
(73) Dikovskaya, D.; Schiffmann, D.; Newton, I. P.; Oakley, A.; Kroboth, K.; Sansom, O.; Jamieson, T. J.; Meniel, V.; Clarke, A.; Näthke, I. S. Loss of APC Induces Polyploidy as a Result of a Combination of Defects in Mitosis and Apoptosis. *J. Cell Biol.* **2007**, *176* (2), 183−195.
(74) Oloumi, A.; McPhee, T.; Dedhar, S. Regulation of E-Cadherin Expression and β-Catenin/Tcf Transcriptional Activity by the Integrin-Linked Kinase. *Biochim. Biophys. Acta - Mol. Cell Res.* **2004**, *1691* (1), 1−15.
(75) Huang, T.; Chen, Q. F.; Chang, B. Y.; Shen, L. J.; Li, W.; Wu, P. H.; Fan, W. J. TFAP4 Promotes Hepatocellular Carcinoma Invasion and Metastasis via Activating the Pi3k/Akt Signaling Pathway. *Dis. Markers* **2019**, *2019*, 1.
(76) Chaffer, C. L.; San Juan, B. P.; Lim, E.; Weinberg, R. A. EMT, Cell Plasticity and Metastasis. *Cancer Metastasis Rev.* **2016**, *35* (4), 645−654.
(77) Yang, S.; Chen, J.; Tan, T.; Wang, N.; Huang, Y.; Wang, Y.; Yuan, X.; Zhang, P.; Luo, J.; Luo, X. Evodiamine Exerts Anticancer Effects against 143b and Mg63 Cells through the Wnt/β-Catenin Signaling Pathway. *Cancer Manag. Res.* **2020**, *12*, 2875−2888.


https://doi.org/10.1021/acsomega.3c02732
*ACS Omega* 2023, 8, 43474−43489